The Response of Simulated Nocturnal Convective Systems to a Developing Low-Level Jet

ADAM J. FRENCH AND MATTHEW D. PARKER

Department of Marine, Earth, and Atmospheric Sciences, North Carolina State University, Raleigh, North Carolina

(Manuscript received 21 September 2009, in final form 21 April 2010)

ABSTRACT

Some recent numerical experiments have examined the dynamics of initially surface-based squall lines that encounter an increasingly stable boundary layer, akin to what occurs with the onset of nocturnal cooling. The present study builds on that work by investigating the added effect of a developing nocturnal low-level jet (LLJ) on the convective-scale dynamics of a simulated squall line. The characteristics of the simulated LLJ atop a simulated stable boundary layer are based on past climatological studies of the LLJ in the central United States. A variety of jet orientations are tested, and sensitivities to jet height and the presence of low-level cooling are explored.

The primary impacts of adding the LLJ are that it alters the wind shear in the layers just above and below the jet and that it alters the magnitude of the storm-relative inflow in the jet layer. The changes to wind shear have an attendant impact on low-level lifting, in keeping with current theories for gust front lifting in squall lines. The changes to the system-relative inflow, in turn, impact total upward mass flux and precipitation output. Both are sensitive to the squall line–relative orientation of the LLJ.

The variations in updraft intensity and system-relative inflow are modulated by the progression of the low-level cooling, which mimics the development of a nocturnal boundary layer. While the system remains surface-based, the below-jet shear has the largest impact on lifting, whereas the above-jet shear begins to play a larger role as the system becomes elevated. Similarly, as the system becomes elevated, larger changes to system-relative inflow are observed because of the layer of potentially buoyant inflowing parcels becoming confined to the layer of the LLJ.

1. Introduction

Warm season precipitation has long been observed to exhibit a nocturnal maximum over the central United States (e.g., Kincer 1916), which has been attributed to a preponderance of nighttime thunderstorms and mesoscale convective systems (MCSs) that cross the region (e.g., Wallace 1975; Maddox 1980). While these MCSs benefit agriculture by supplying a significant portion of the growing-season rainfall in this region (Fritsch et al. 1986), they can also cause flooding (Doswell et al. 1996) and severe weather (Gallus et al. 2008), with associated concerns for life and property. In light of this, nocturnal MCSs have been the focus of a variety of studies, using both observations (e.g., Maddox 1980, 1983; Wetzel et al. 1983; Goodman and MacGorman 1986; Cotton et al. 1989; Carbone et al. 1990; Trier and Parsons 1993; Gale et al. 2002) and numerical simulations (e.g., Dudhia et al. 1987; Schmidt and Cotton 1990; Buzzi et al. 1991; Trier et al. 2006).

Determining the processes that sustain these convective systems in a nocturnal environment featuring a statically stable lower troposphere has been of particular interest. To this end, Parker (2008, hereafter P08) examined the effect of low-level (i.e., the lowest 1 km) cooling on simulated squall lines, focusing on the convective-scale dynamical processes. He found that as the convective system transitioned from surface-based (ingesting parcels from approximately the lowest 500 m) to elevated (ingesting parcels from above approximately 500 m), the mechanism responsible for lifting inflowing parcels evolved from a cold pool to a bore. In the interest of simplicity, the simulations of P08 utilized a homogeneous background wind profile that did not include a low-level wind maximum, or low-level jet (LLJ), which is commonly observed in nocturnal MCS environments (e.g., Maddox 1983; Cotton et al. 1989). While numerous previous studies have highlighted the importance of the

Corresponding author address: Adam French, North Carolina State University, Campus Box 8208, Raleigh, NC 27695–8208.
E-mail: ajfrench@ncsu.edu

DOI: 10.1175/2010JAS3329.1

LLJ as a forcing mechanism and as a means of transporting high-θ_e air into the region where storms are occurring, few have examined how the development of the jet impacts the dynamics of pre-existing convection. The present work looks to fill in this gap in the knowledge base by focusing on how a developing LLJ effects simulated nocturnal convective systems, namely those with a linear organization such as squall lines.

Background

A primary reason that the LLJ is of interest is its long-standing association with warm-season precipitation in the central United States, particularly thunderstorms (e.g., Means 1952; Pitchford and London 1962; Higgins et al. 1997). Given its location and typical southerly direction, the LLJ is a significant source of instability for the central United States because it advects warm, moist air from the Gulf of Mexico northward into the Great Plains and the Midwest (Helfand and Schubert 1995; Higgins et al. 1997; Tollerud et al. 2008). This warm, moist air is often potentially buoyant and can provide the sustaining inflow for convective storms (Maddox 1983; Cotton et al. 1989). The LLJ can also destabilize a region when its associated ribbon of high-θ_e air underruns colder air aloft, leading to either potential or conditional instability that, when released, fuels storm development (Trier and Parsons 1993). Additionally, the jet can locally deepen the moist layer via strengthening isentropic lift and frontogenetic circulations in cases where the jet interacts with deep thermal boundaries (Trier et al. 2006). These effects can be especially significant for nocturnal convection or storms that form on the cool side of frontal boundaries, as the LLJ provides an elevated source of unstable air upon which storms can be sustained despite the stable boundary layer (Trier et al. 2006).

In addition to helping prime the convective environment, the LLJ can also provide a significant forcing mechanism for long-lived convective systems. This is especially true when the jet intersects a frontal boundary (Pitchford and London 1962; Augustine and Caracena 1994; Anderson and Arritt 1998). As the jet impinges upon the frontal boundary, isentropic upglide and frontogenetic forcing are enhanced, leading to a local increase in vertical motion and providing a lifting mechanism for storms (Trier and Parsons 1993; Tuttle and Davis 2006; Trier et al. 2006). This forcing can be important to storm longevity during the overnight hours. In a study examining MCS dissipation, Gale et al. (2002) noted that not only was an LLJ present in a majority of their cases, but that storm dissipation often corresponded to the removal of the LLJ forcing. This was often the result of the jet becoming oriented more parallel to the front, resulting in a decrease in isentropic upglide and frontogenetic forcing for vertical motion. The authors attributed this change in direction to the diurnal inertial oscillation. In the absence of a frontal boundary, upward vertical motion associated with speed convergence at the terminus of the jet (Trier and Parsons 1993) or interactions between the LLJ and a pre-existing mesoscale convective vortex (Schumacher and Johnson 2009) are also capable of initiating and sustaining MCSs. As a forcing mechanism, the strength of the LLJ also has significant implications for MCS intensity. Tuttle and Davis (2006) found that stronger jets were associated with heavier rainfall. This corresponds with the findings of Arritt et al. (1997), who concluded that an increased frequency of *strong* LLJs may have played a role in the significant flooding that occurred across the Midwestern United States in 1993.

Finally, given this role as a forcing mechanism for MCSs, Corfidi et al. (1996) developed a method for forecasting the motion of mesoscale convective complexes (MCCs) that included using the LLJ as a proxy for the propagation component of storm motion. Quite simply, storm propagation is represented by a vector equal in magnitude but opposite in direction to the LLJ. A refinement of this study (Corfidi 2003) noted that this proxy does not work as well for cold-pool-driven systems that move downwind and is instead more applicable to systems that propagate upwind, such as the ''backbuilding'' mode of Bluestein and Jain (1985) or the quasi-stationary/backbuilding mode of Schumacher and Johnson (2005).

In short, a significant body of work has been compiled outlining the role of the LLJ as an environmental feature associated with large, long-lived MCSs. However, much of this work has focused either on the role that the jet plays in priming the convective environment (i.e., transporting high-θ_e air to the region where storms are occurring) or on storms that develop as a direct result of forcing by the jet. Missing from this collection of previous work is an explanation of how the development of the nocturnal jet may affect pre-existing convection (i.e., storms that have formed during the afternoon and continue into the overnight hours as the boundary layer stabilizes and the LLJ develops). Of particular interest is how the LLJ impacts the convective-scale dynamics of these systems. One way that the development of the nocturnal LLJ may impact ongoing storms, particularly squall lines, is through changing the vertical wind shear profile. Given that vertical shear is important for squall line organization and longevity (e.g., Rotunno et al. 1988, hereafter RKW), changes to the vertical shear due to the developing LLJ are hypothesized to be important to the evolution of these systems. In addition, the presence of an LLJ may also govern the intensity of the storm-relative

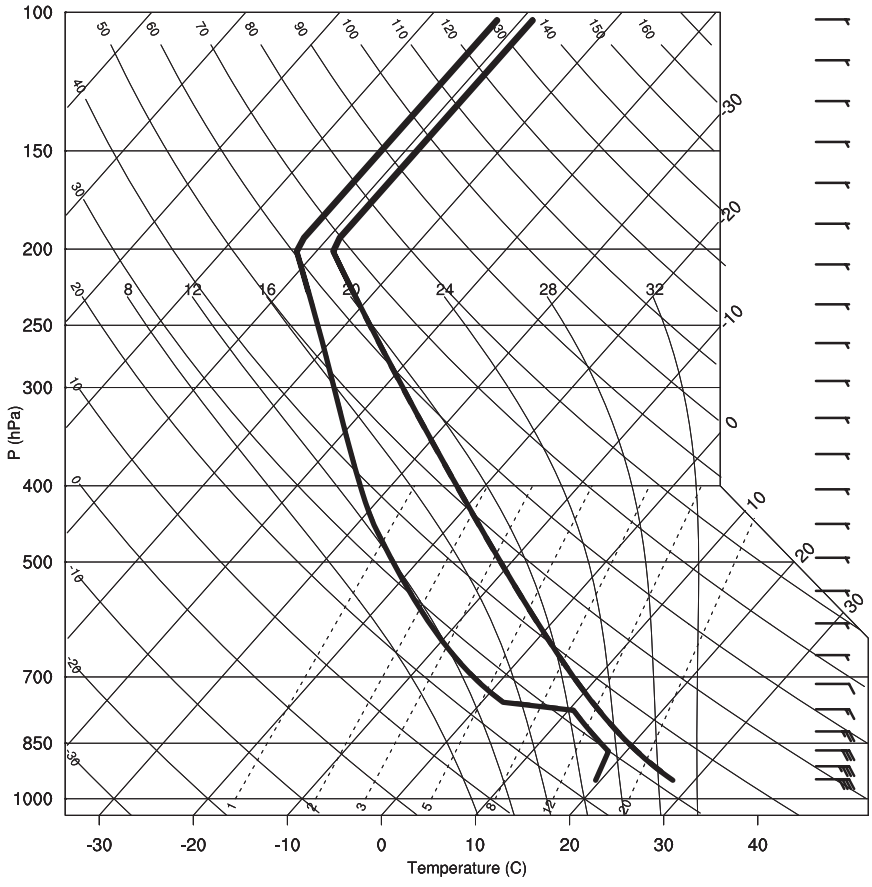

FIG. 1. Skew T–ln$p$ diagram of the base-state temperature and dewpoint (thick black lines) and wind (barbs, half and full barbs = 2.5 and 5 m s^{-1}, respectively) profiles for all simulations.

inflow that sustains a squall line, which can directly impact storm intensity (Gale et al. 2002).

The present work looks to examine these effects using idealized numerical simulations. The following section provides an overview of the methods used in this study. This is followed in section 3 by a discussion of the results of a set of simulations that utilize periodic-y boundary conditions. Section 4 details the results of a variety of sensitivity tests, and section 5 examines the impact of adding the jet to a nonperiodic squall line. These results are synthesized in section 6, leading up to a summary and conclusions in section 7.

2. Methodology

This work utilized 3D idealized numerical model simulations using version 1.10 of the Bryan cloud model (CM1) described by Bryan and Fritsch (2002). To compare our results to previous work, our model configuration followed that of P08. This included using the Lin et al. (1983) ice microphysics scheme [with the modifications of Braun and Tao (2000) included] and a 250-m horizontal grid spacing to explicitly represent convective processes. The vertical grid spacing was stretched from 100 m at the surface to 250 m above $z = 2500$ m. This provided higher resolution in the lower troposphere, where both a nocturnal stable layer and the simulated LLJ were located. The 3D simulations used a $400 \times 60 \times 20$ km domain with periodic-y (along-line) and open-x lateral boundary conditions. Finally, we employed free-slip upper and lower boundary conditions, with a Rayleigh damping layer above 14 km. In the interest of simplicity, accelerations due to the Coriolis force, as well as any radiative effects, were neglected. This basic model configuration was used for the majority of our simulations; any changes for subsequent tests will be noted where applicable. All of the simulations were run for 10 h.

As in P08, the guiding philosophy is to mimic the transition of afternoon storms as night falls. The base-state environment employed for these simulations was the same horizontally homogeneous environment used in P08 (Fig. 1), utilizing the mean midlatitude MCS sounding with a deepened moist layer from Parker and Johnson (2004, hereafter PJ04). This deeper moist layer is

representative of an environment that supports surface-based storms but also contains an elevated layer of high-θ_e air, which is necessary to sustain an MCS in an environment with a stable boundary layer. In the central United States, this air is commonly fluxed into place by the LLJ; for simplicity, we assume that the higher-θ_e layer is already present, so that the dynamical impact of the LLJ is isolated to the changing wind profile. Convection was initiated within this environment using a 10-km wide, 3-km deep, north–south line thermal that spanned the domain in the *y* direction. This initial perturbation was 2 K warmer than the background environment, had a relative humidity of 85%, and featured random temperature perturbations of up to 0.1 K to help facilitate 3D structures.

Artificial low-level cooling was introduced in the simulations using much the same method as that used by P08. In P08, the simulated squall lines were allowed to mature for 3.0 h after which a simplified low-level cooling term was added in the lowest 1 km of the model. The net effect of this cooling was to create an isothermal layer whose temperature decreased from the initial surface temperature at a rate of 3 K h^{-1}. This approach is again adapted in the present study as a simple way of enabling convection to mature in an afternoon-like sounding and then to evolve as a nocturnal-like sounding develops. The cooling is applied only at those grid points whose temperature exceeds the temporally declining isothermal reference temperature. In the present study the isothermal reference temperature decreases indefinitely, making the cooling configuration the same as the ''-unlim'' experiments of P08.

When such cooling is applied indefinitely, a fog will eventually form in the low-level environment, a situation that is not handled well by the model's idealized microphysical parameterization. Therefore, P08 reported that at grid points where the artificial cooling was applied, the relative humidity (RH) was reset to be no larger than 0.98 through the instantaneous removal of water vapor (without any latent heat release). In the course of extending the work of P08 via some new experiments, we discovered (a) that a number of the simulations described by P08 actually used an older version of the artificial cooling scheme that did not include the RH treatment and (b) that the RH treatment, as it was implemented in the remaining simulations, appears to have some undesirable effects. These problems were attributable to a coding error introduced by P08 and are not general problems with the standard distribution of the Bryan cloud model. The ramifications of these deficiencies are discussed in more detail in the appendix. In revisiting the original P08 simulations to determine the sensitivity of the results to the RH correction, we have developed a revised technique that is much preferred to the one described by P08.

In the revised version, the artificial cooling routine has been moved so that it occurs at the end of the model microphysical parameterization instead of during the model's main prediction of potential temperature computations. This allows the model to treat moist processes associated with the model's simulated physical processes first, before the artificial cooling is introduced. As a result of this improvement, it was then possible simply to add the artificial cooling and remove any induced supersaturation, resetting RH to be no larger than 1.00 and allowing no condensation during the artificial cooling step. This revised technique is preferable to the original and has been applied uniformly to all of the present simulations. The modest impacts of this revision on the results of P08 are addressed in the appendix.

To study the effects of an LLJ on nocturnal convective systems, it was of interest to include a developing low-level wind maximum within these simulations. A review of past LLJ climatologies (Bonner 1968; Mitchell et al. 1995; Arritt et al. 1997; Whiteman et al. 1997) provided the basis for our simulated LLJ. This included using a jet that was 5 m s^{-1} stronger than the background winds,[1] approximately 1 km deep, and centered just above the developing stable layer (in our case, just above 1 km AGL). As is often observed (Mitchell et al. 1995) our jet gradually develops over the course of 5.0 h (beginning 3.0 h into the simulation, the same time as the onset of the low-level cooling) resulting in the perturbation wind profile shown in Fig. 2a. This profile features a rapid increase in wind with height to the maximum jet speed followed by a gradual relaxation back to the base state profile above this level, similar to the LLJ wind profiles observed by Whiteman et al. (1997) and Tollerud et al. (2008). While several climatologies (e.g., Bonner 1968; Whiteman et al. 1997; Song et al. 2005) place the level of maximum winds within the jet below the 1-km AGL level used in our simulations, they also point out that the jet tends to be located just above the top of the nocturnal stable layer. Since the latter of these would appear more dynamically relevant, for our primary simulations we chose to place our jet relative to the top of our imposed stable layer rather than at a specific height. Finally, three different jet orientations relative to the squall line's leading line were tested; rear-to-front (RTF), front-to-rear (FTR), and parallel (PAR) (Fig. 2b). These simulations were compared to a control simulation (CTL) that did

[1] Stronger jet speeds were tested as well and did not fundamentally change our results. Jet-induced changes were of the same sign, just larger in magnitude for a stronger jet.

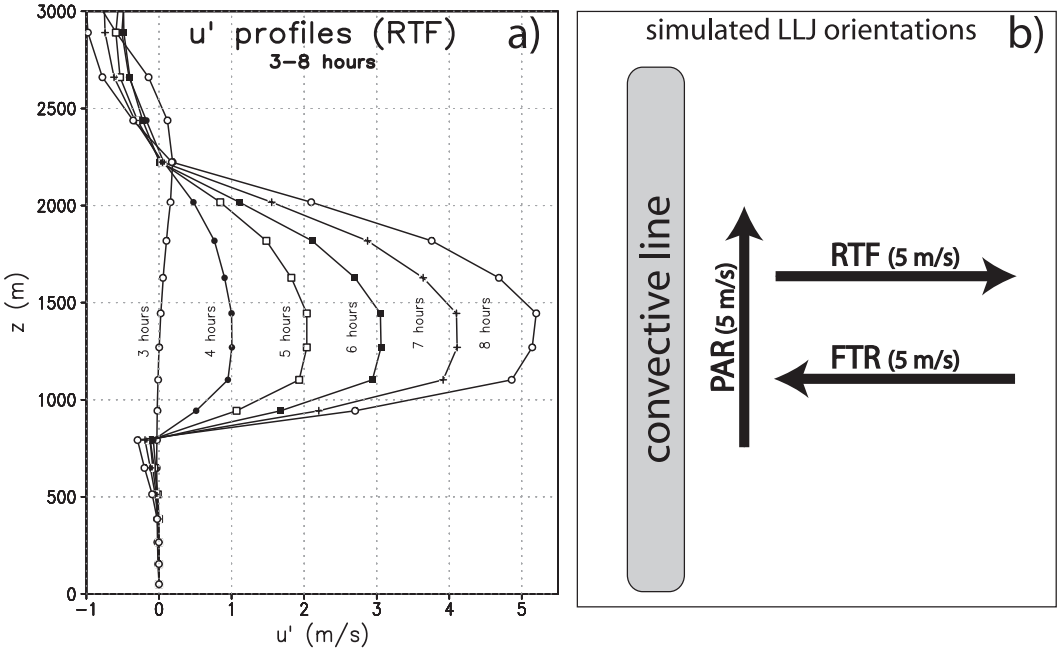

FIG. 2. (a) Time series of perturbation *u*-wind profiles illustrating the development of the simulated LLJ. (b) Schematic illustrating the different LLJ orientations. The wind profiles in (a) are from RTF simulation. The other jet orientations have an identical shape and magnitude but a different direction.

not include any jet development and was therefore identical to the ''deep-unlim'' simulation of P08.

It should be noted that our applied LLJ is a jet in the vertical only, as it is applied uniformly across our domain in the *x* and *y* directions. In addition, we do not limit the jet application to the undisturbed environment ahead of the squall line but rather apply it at every point in the *x* and *y* directions, which includes points within our simulated squall line. This was done to avoid introducing additional convergence within the model at the jet terminus and thus isolating the jet as a characteristic of the larger (meso-beta/alpha) scale environment rather than a forcing mechanism for our simulated squall line. There is little evidence of the applied *u* perturbations within the squall line structure, likely owing to strong vertical motions effectively mixing the narrow maximum with the surrounding wind field. Furthermore, we ran several 2D tests wherein the jet was limited to the preline region of the model domain and found that the primary impact was that storm motions were more uniform across the simulations. Overall, key features and storm evolutions remained unchanged, giving us confidence that our results are robust.

3. Benchmark simulations

a. Overview of simulations

To test the effects of adding a basic LLJ structure to the simulations of P08, we first varied the jet orientation with respect to the simulated linear MCS. An examination of the CTL, FTR, RTF, and PAR (not shown) simulations shows a fairly similar evolution through 6.0 h of run time (Fig. 3). In each case, an initially surface-based squall line develops and becomes elevated as is illustrated in Fig. 4 for the CTL simulation. The shaded tracer in Fig. 4 denotes low-level parcels being ingested by the squall line, with a decrease in tracer denoting the transition from surface-based to elevated convection as the surface temperature decreases and low-level CAPE tends to 0 J kg^{-1} (left- and right-hand panels, respectively, of Fig. 4). As discussed in P08, the life cycle of the CTL squall line is characterized by a developing stage as the squall line intensifies between 0.0 and 3.0 h, a mature–steady phase between 3.0 and 6.0 h while the squall line is surface-based, a transitional stage as the squall line evolves from surface-based to elevated between 6.0 and 8.0 h (the ''stalling phase'' discussed in P08), and finally the elevated stage wherein the squall line is only ingesting parcels from above the boundary layer. All of the simulations steadily diminish in intensity with time (e.g., Figs. 3 and 5) because of dwindling preline CAPE values in response to the low-level cooling. This evolution was discussed at length by P08, and given that all three jet simulations largely mimic the CTL simulation in this progression, the reader is referred to that publication for more detail.

The observed similarity is maintained between CTL and PAR for the duration of the simulations (not shown),

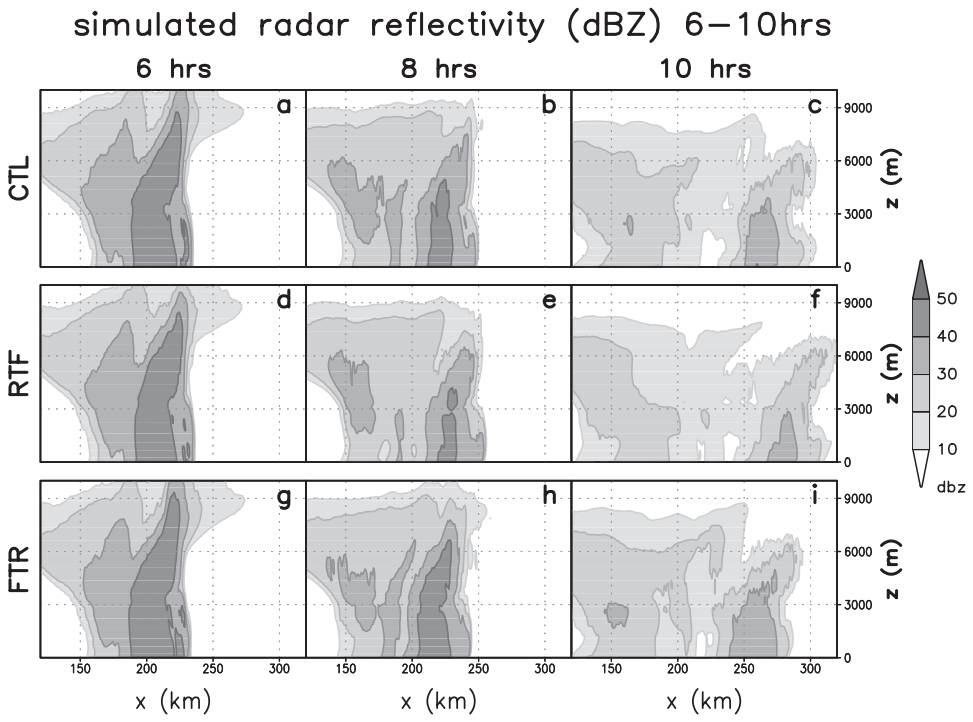

FIG. 3. Vertical cross sections of simulated radar reflectivity (dBZ, shaded) for the (a)–(c) CTL, (d)–(f) RTF, and (g)–(i) FTR simulations at (left to right) $t = 6.0$, 8.0, and 10.0 h.

suggesting that for the case of periodic-y boundary conditions, a line-parallel LLJ has little effect on the simulated squall line. In light of this, subsequent discussions will focus solely on the line-perpendicular jet orientations (RTF and FTR), as these produced more dramatic changes from CTL. An analysis of the impacts of the PAR configuration using nonperiodic boundary conditions and a finite length squall line are discussed in section 5.

In general, the CTL, FTR, and RTF simulations are qualitatively similar through approximately 6.0 h, at which point the region of higher reflectivity in the RTF simulation begins to diminish at a faster rate compared to the CTL and FTR simulations (Fig. 3). By the end of the simulation (10.0 h), reflectivity values have decreased in all three of the simulations, but the FTR run continues to exhibit a larger area of >40 dBZ simulated radar reflectivity than the CTL run, while this area is considerably smaller in the RTF simulation. A more quantitative examination of the evolution during this period is evident using the total upward mass flux (TUMF; Fig. 5a). Starting at approximately $t = 3.5$ h (30 min after the onset of low-level cooling and LLJ application), the FTR simulation begins to exhibit larger TUMF than the CTL simulation, while the TUMF becomes slightly smaller in the RTF run. This pattern is maintained throughout the duration of the simulation. This suggests that the addition of the LLJ very quickly leads to an increase in total upward mass flux in the FTR simulation, which eventually manifests itself in a prolonged duration of stronger precipitation compared to the RTF simulation, as is evident in the simulated radar reflectivity (Fig. 3).

A time series of the maximum along-line averaged vertical velocity $[\overline{w}]_{\max}$ indicates that updraft evolution is not as straightforward (Fig. 5b). By approximately 4.0 h (1.0 h after the onset of the low-level cooling and LLJ application) the RTF and FTR simulations begin to diverge from the CTL simulation. The RTF simulation develops stronger updrafts while the FTR updrafts remain weaker (and shallower; not shown). This discrepancy increases until approximately $t = 5.5$ h at which point the RTF simulation has along-line averaged vertical velocity ($\overline{w}$) that is 2 m s^{-1} stronger than the FTR (Figs. 6b,c). In addition, both the RTF and CTL simulations feature unbroken regions of strong (>5 m s^{-1}) vertical velocities extending approximately 1 km deeper than in the FTR simulation (dashed contours in Fig. 6). This suggests weaker low-level lifting occurring in the FTR simulation during this period compared to both the RTF and CTL simulations. This trend reverses between approximately $t = 6.0$ and 8.0 h, (Fig. 5b). The updrafts in the RTF simulation begin a steady decline in intensity and depth, whereas those in the FTR remain nearly steady in intensity and begin to deepen. The three simulations are comparable by $t = 6.75$ h (e.g., Fig. 5b), and

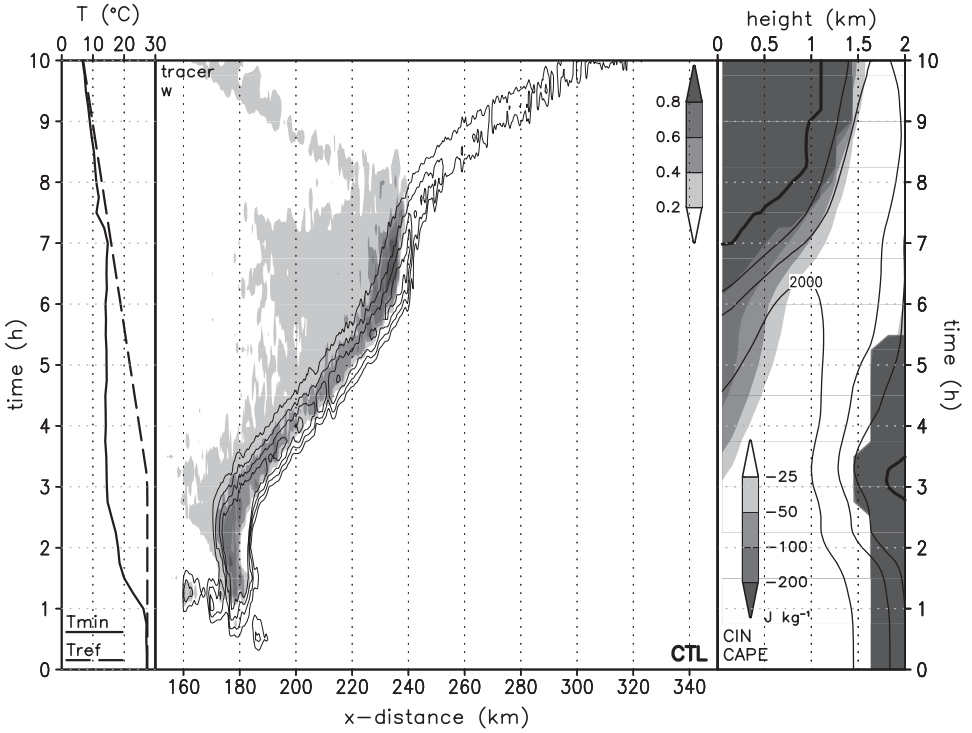

FIG. 4. Depiction of the CTL simulation over time: (left) values vs time for the reference environmental temperature (Tref) and the minimal surface temperature on the domain (Tmin), using line styles as shown; (center) Hovmöller diagram for 5 km AGL, with along-line maxima in tracer concentration (shaded) and vertical velocity (contoured at 10, 15, 20, and 25 m s^{-1}); (right) vertical profile of environmental CIN (shaded) and CAPE (contoured at 500, 1000, and 2000 J kg^{-1}, with bold contour at 0 J kg^{-1}) vs time. The ordinate for all three panels is time.

by $t = 7.5$ h the FTR simulation has surpassed both the CTL and RTF in updraft intensity (nearly twice the intensity of the RTF) with strong $\overline{w}$ extending to a higher altitude than both CTL and RTF (Fig. 7). Lastly, after about $t = 7.5$ h a final evolution takes place, as $[\overline{w}]_{\max}$ values in the FTR squall line weaken rapidly, while those in the RTF slow in their decrease (Fig. 5b), and the simulations' $[\overline{w}]_{\max}$ values become quite similar again. However, the low-level structure varies considerably during this period, with the RTF exhibiting a narrow, erect updraft, while the FTR features a broader, rearward sloping structure (Fig. 8). The reasons for these comparative changes are explored next.

b. Role of changes to the low-level wind shear

One way in which the development of a low-level jet can impact a squall line is by changing the vertical wind shear of the preline environment, which can have a significant impact on the strength of vertical motion within the squall line. As presented by RKW, lifting along a squall line's cold pool is optimized when the cold pool strength C (a measure of integrated buoyancy within the cold pool) is balanced by the environmental wind shear in the preline region Δu. The physical interpretation of this balance is that the negative horizontal vorticity produced baroclinically by the cold pool is balanced by the positive horizontal vorticity flux associated with the vertical wind shear, resulting in vertically erect, intense updrafts. This concept has been demonstrated repeatedly in numerical simulations of squall lines (e.g., Weisman et al. 1988; Weisman and Rotunno 2004; Bryan et al. 2006; P08) and, given the changes to the vertical shear that result from our addition of an LLJ, it is of interest to examine our simulations in terms of this cold pool–shear balance. As shown by P08, in the CTL simulation the cold pool is stronger than the shear to begin with, and thus we assess increases in vertical shear as bringing the system closer to balance and decreases in shear as taking the system further from balance.

RKW and a more recent study by Weisman and Rotunno (2004) utilize a layer of fixed depth in assessing the impact of the environmental shear (e.g., 0–2.5 km AGL). The general logic behind this treatment is that (a) the shear and the cold pool's buoyancy perturbation do

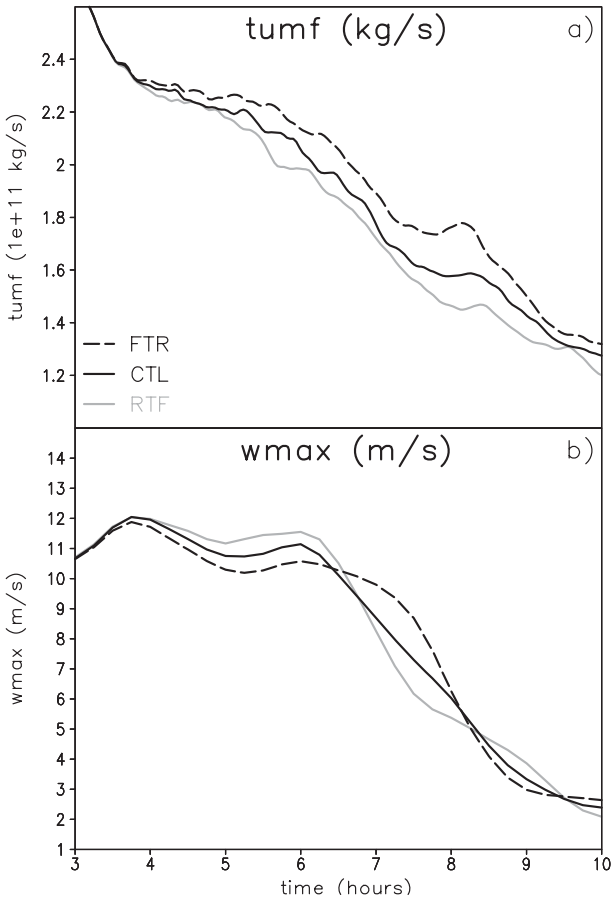

FIG. 5. Time series of (a) TUMF (kg), and (b) $[\overline{w}]_{\max}$ (m s^{-1}) from $t = 3.0$ to 10.0 h for the RTF (gray solid), FTR (dashed), and CTL (black solid) simulations.

not vary appreciably with height in the layer and (b) the shear in the layer containing the cold pool is of greatest importance. The combination of these two assumptions leads to an elegant approach in which the cold pool's buoyancy and environment's flux of horizontal vorticity can be integrated and compared via the proxies C and Δu. However, in the present study taking a simple vector wind difference over the 0–2.5-km AGL layer, for example, does not capture the impacts of our LLJ on the preline shear because the jet is contained almost entirely within this layer. As a result, the 0–2.5-km vertical wind shear values in the RTF and FTR simulations are nearly identical to those found in the CTL simulation (Table 1).

While assessing the appropriateness of the preceding assumptions for our LLJ experiments, we noted that the layer of strongly negative and nearly constant buoyancy in our own cold pool extended up through approximately 1 km AGL (e.g., left-hand panels of Fig. 6). This also nearly coincides with the height of the imposed LLJ's

TABLE 1. Vector wind differences for the 0–2.5, 0–1, 1–2.5, and 0.5–1.5 km AGL layers for CTL, RTF, and FTR simulations at $t = 8.0$ h.

Layer (km)	CTL (m s^{-1})	RTF (m s^{-1})	FTR (m s^{-1})
0–2.5	13.64	13.99	13.45
0–1	5.32	8.08	2.64
1–2.5	8.32	5.91	10.85
0.5–1.5	5.49	10.90	0.27

wind maximum. We therefore find it most instructive to separate the 0–1- and 1–2.5-km layers (because of their differing cold pool buoyancy and environmental shears). This separation at 1 km is also convenient because, once the artificial cooling is applied, the air parcels below 1 km AGL have escalating amounts of convective inhibition (CIN) and, eventually, vanishing CAPE (Figs. 9a,b). In the original formulation of RKW (e.g., their p. 477), the horizontal vorticity equation is integrated vertically. It seems to us that the integrated horizontal vorticity tendencies should be determined by the relationship of the (horizontal gradients in) environmental horizontal vorticity flux to the cold pool's buoyancy *in the layer where the cold pool buoyancy and its horizontal gradient are maximized.* It also seems to us that once parcels no longer have CAPE (i.e., in the layer of 0–1-km artificial cooling), they should be excluded from the problem (because they no longer take part in deep convection). These hypotheses underlie our approach to assessing the impact of shear on our simulations, using the 0–1- and 1–2.5-km layers throughout for simplicity.

Over the 0–1-km layer the RTF jet results in an increase in vertical shear from the base state (CTL) environment (Table 1), which better balances the cold pool (found predominantly in that layer; Fig. 6). This is associated with an increase in $[\overline{w}]_{\max}$ during the surface-based phase ($t = 3.0$–6.5 h), as is seen in Fig. 5b. Meanwhile, the FTR jet reduces the vertical shear in the 0–1-km layer, which is concurrent with the decreased $[\overline{w}]_{\max}$ in Fig. 5b. In short, while the squall line is surface based, the below-jet shear is well correlated to the peak vertical motions in our simulations.

Shortly after 6.0 h the simulated squall lines enter the stalling phase, which is characterized by a weakening of the surface cold pool and a secondary maximum in vertical velocity as discussed by P08. With the addition of the LLJ, this phase marks the start of a period of comparatively strong vertical velocities in the FTR simulation. As the squall line enters the stalling phase, several things happen simultaneously. First, as the stable layer continues to cool, the temperature difference across the cold pool's gust front weakens (Figs. 7 and 9c), and the strength of lifting by the cold pool diminishes. This

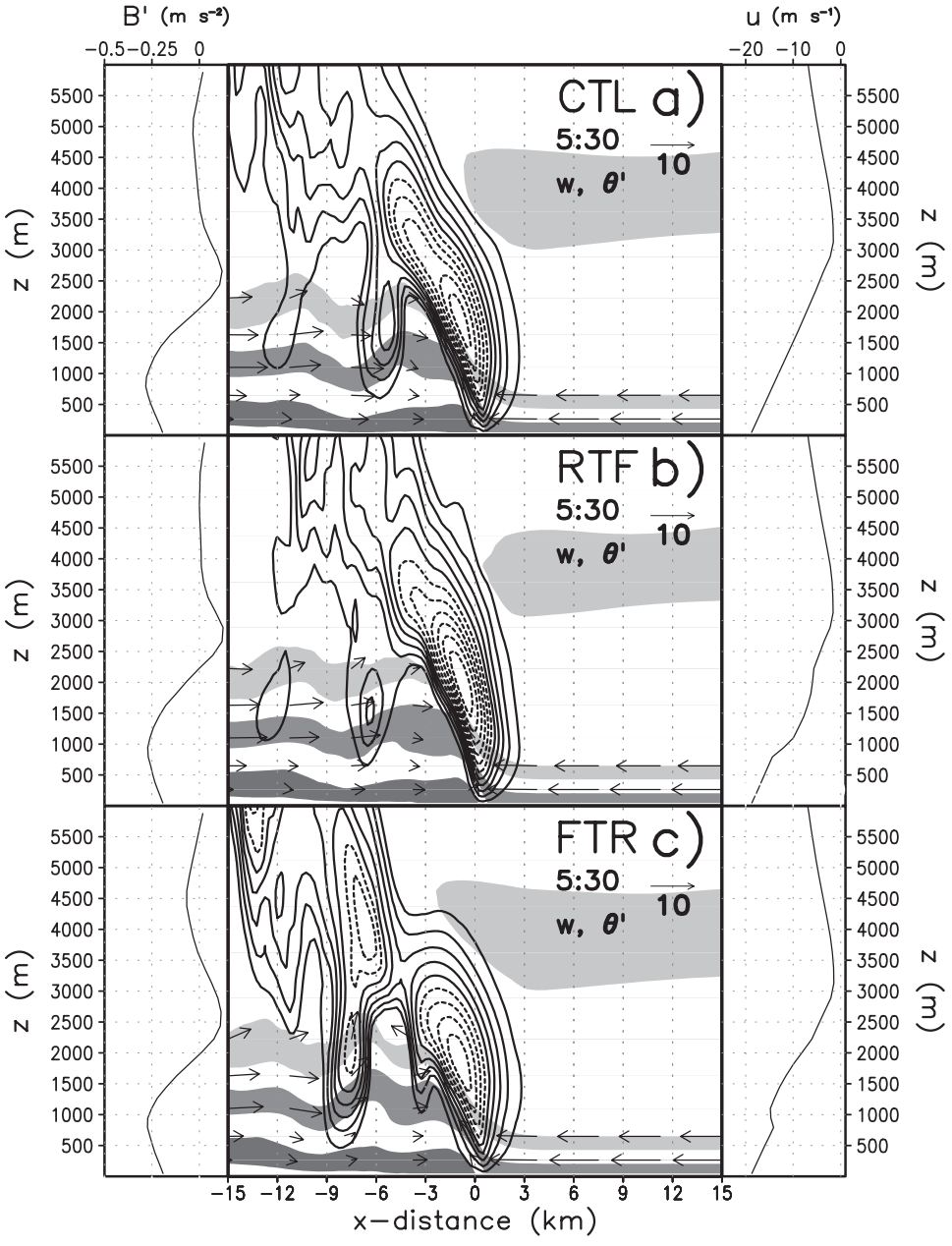

FIG. 6. Assorted fields for (a) CTL, (b) RTF, and (c) FTR simulations at $t = 5.5$ h: (center) vertical cross section of $\overline{w}$ (contoured, dashed contours > 5 m s^{-1}), potential temperature perturbation (θ', alternately shaded every 2 K below -2 K), and wind vectors within the developing stable layer and cold pool (m s^{-1}, scale vector at upper right); (right) along-line averaged u-wind profile at $x = 390$ km (well ahead of the squall line); (left) along-line averaged buoyancy perturbation (relative to the evolving preline environment) 1 km behind the system gust front.

happens first at low levels, where the air is colder, and then extends upward (Fig. 9c). At the same time, continued cooling of the stable layer continues to reduce CAPE and increase CIN (Figs. 9a,b). Again, this effect is largest at low levels and extends upward with time. The combined impacts of the low-level weakening of the cold pool and increasing preline stabilization cause the layer of potentially buoyant parcels feeding the squall line to shift upward with time. Figure 9a also illustrates that CAPE for parcels above approximately 1500 m tends to increase in time. We attribute this to the presence of low-frequency gravity waves generated by the squall

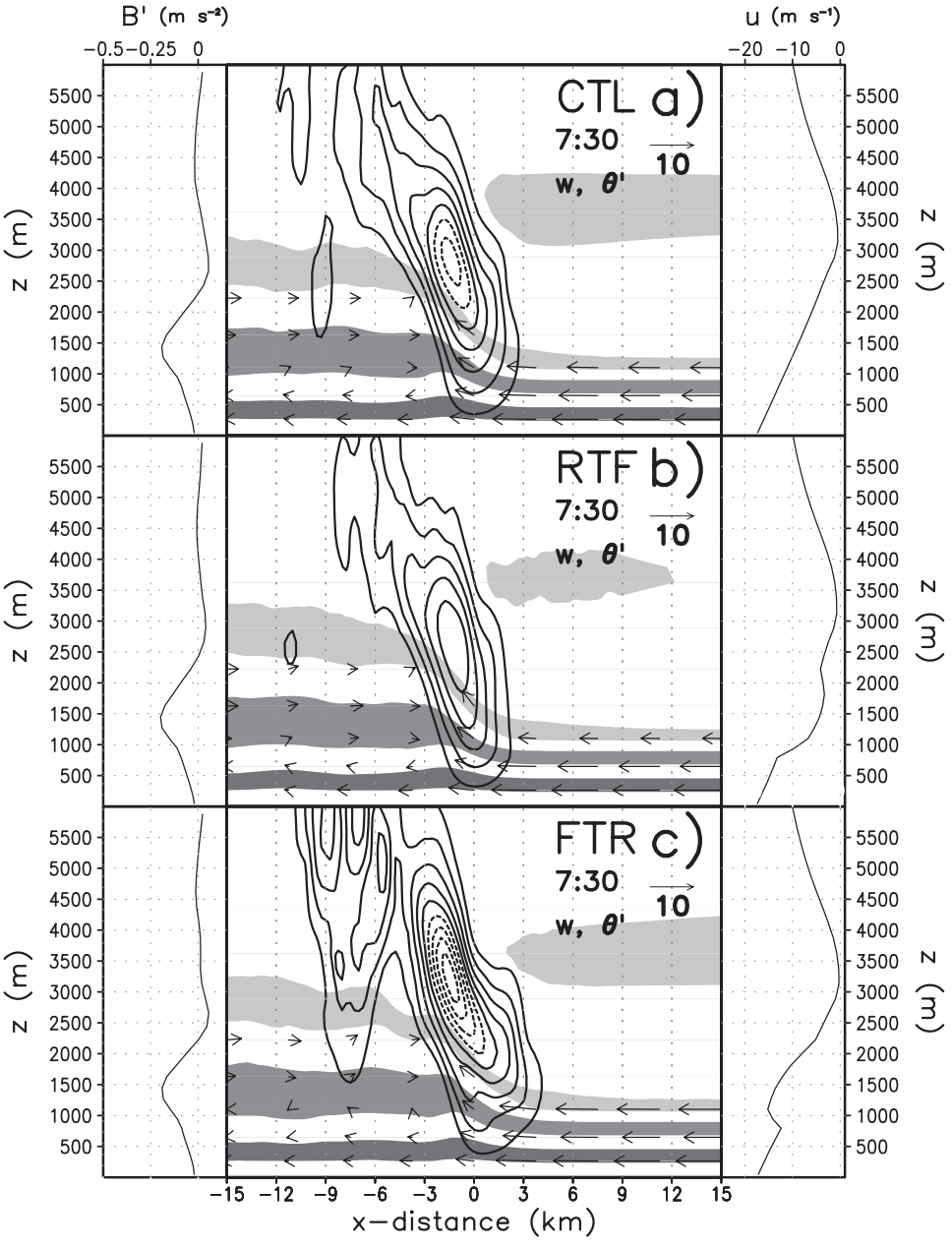

FIG. 7. As in Fig. 6, but at $t = 7.5$ h.

line, which were also observed and explained at length in P08 (1336–1337). As a result of these combined effects, the above-jet wind profile begins to have an increasing impact on the squall line. This results in the FTR squall line producing stronger vertical velocities than the CTL and RTF runs, since it has more favorable shear above 1 km (Table 1). In the RTF simulation, a precipitous dropoff in $[\overline{w}]_{\max}$ occurs as the 0–1-km shear wanes in importance since there is very little above-jet shear (e.g., 1–2.5 km AGL; Table 1).

The 0–1- and 1–2.5-km shear layers are pedagogically useful, but it is also worthwhile to assess the actual vertically integrated horizontal vorticity flux in the LLJ simulations because the jet changes both the shear and the system-relative flow magnitude. Figure 10a compares C for the CTL simulation to the vertically integrated horizontal vorticity flux $u\eta|_z$ for the RTF and FTR simulations. Both C and $u\eta|_z$ are integrated over a subjectively determined *effective inflow layer* that is characterized by the union of the strongest

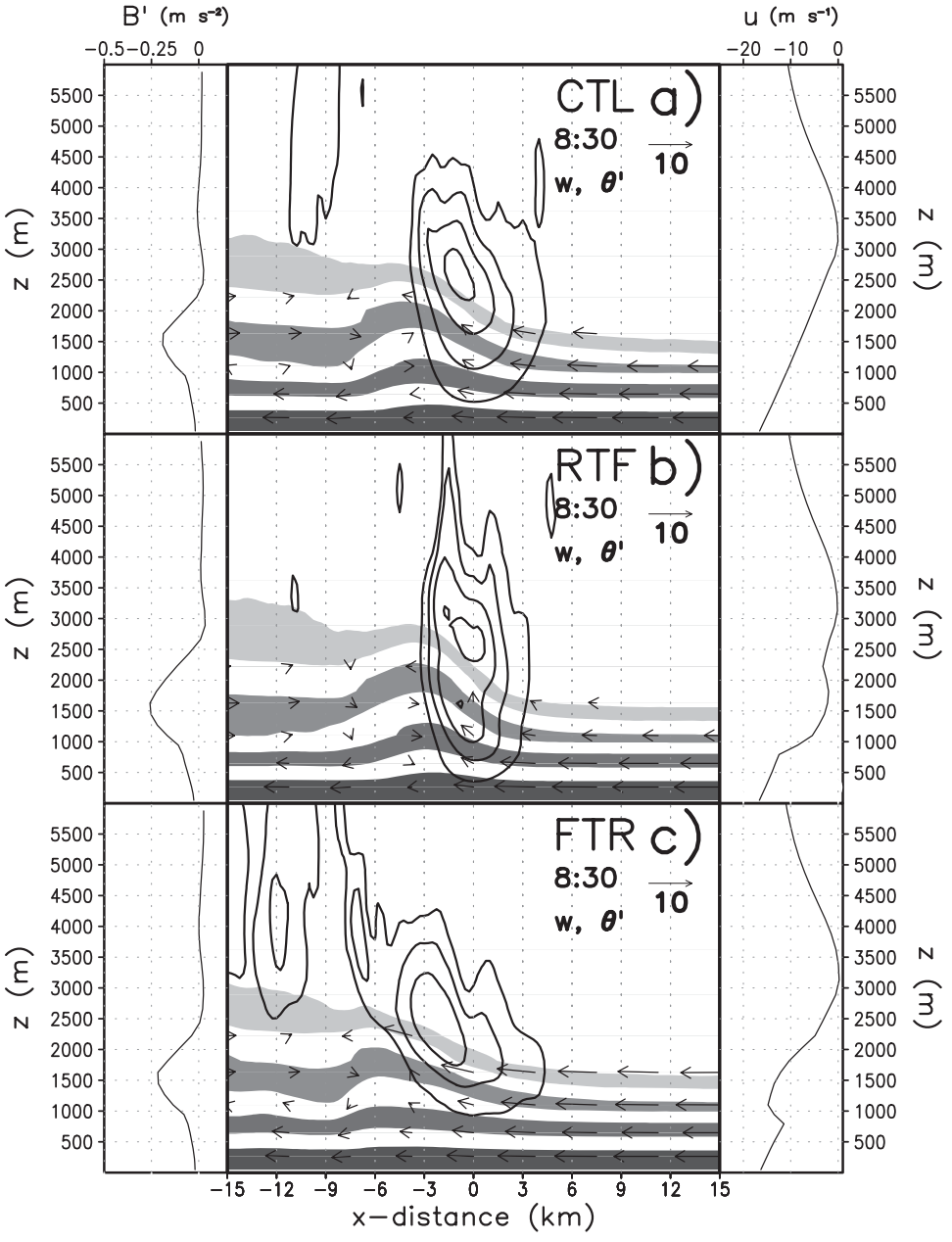

FIG. 8. As in Fig. 6, but at $t = 8.5$ h.

buoyancy perturbation[2] within the cold pool (B') and a preline thermodynamic environment characterized by large CAPE and small CIN (denoted by gray shading in Fig. 9). During the surface-based "steady phase" from $t = 3.0$–6.0 h the below-jet shear predominates, with the RTF (FTR) configuration featuring the most (least) favorable shear (Fig. 10a). This corresponds well with the time evolution of vertical velocity, as the RTF simulation produces the strongest vertical motion during this time (Fig. 5b). From $t = 6.5$–7.5 h as the effective inflow layer shifts upward, the above-jet shear becomes more important, with the FTR jet providing the most favorable conditions (Fig. 10a). This results in the FTR simulation producing the strongest vertical velocities (Fig. 5b), an outcome that is further enhanced because

[2] This perturbation is calculated relative to the changing preline environment to account for the cooling being applied to the inflow environment. Thus it is not a perturbation from the base-state ($t = 0.0$ h) buoyancy field.

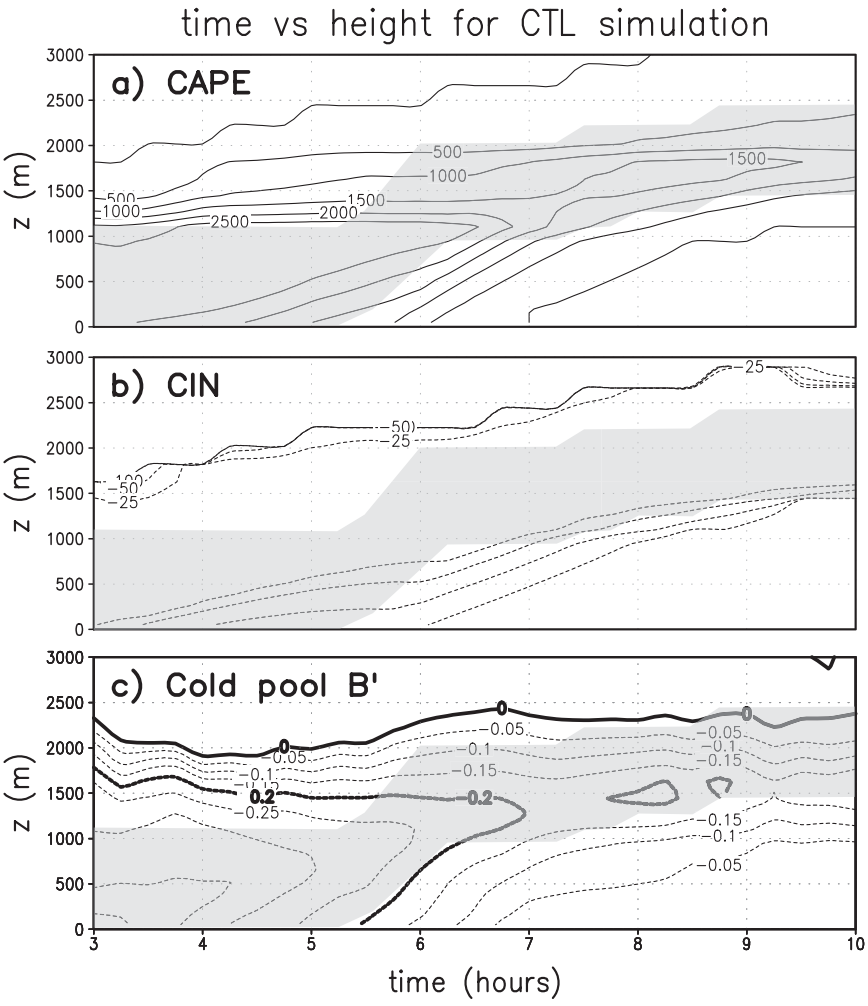

FIG. 9. Time–height plots of along-line averaged (a) CAPE (J kg^{-1}), (b) CIN, and (c) cold pool buoyancy perturbation (B', m s^{-2}) between t = 3.0 and 10.0 h for the CTL simulation. CAPE and CIN are measured at x = 398 km (well ahead of the squall line), while B' is calculated within the cold pool (relative to the evolving preline environment), 1 km behind the gust front. The gray shaded area represents the effective inflow layer discussed in the text.

the cold pool has weakened a great deal by this point (Fig. 10a), and thus the system is closer to the balanced state described by RKW. Meanwhile, since there is very little shear present above the jet in the RTF simulation, its $u\eta|_z$ declines dramatically, and the squall line weakens considerably during this same period.

After approximately t = 7.5 h, as the simulated squall lines become elevated and bore driven (rather than cold pool driven), a final evolution in updraft strength takes place. While all three simulations continue to diminish in updraft intensity, the RTF simulation begins to diminish more slowly, while the FTR hastens its weakening trend (Fig. 5b). Prior to this point, updraft intensity has been well related to the strength of the vertical wind shear within the effective inflow layer, which causes the relevant shear layer to shift upward with time as the depth of the stable layer increases. However, this does not explain the later behavior as the FTR simulation contains the most favorable shear (Fig. 10a) but the weakest updraft (Fig. 8c). Instead, we hypothesize that once the system becomes bore driven, the low-level vertical motions are controlled primarily by the amplitude of the gravity wave/bore. This mechanism can effectively maintain a simulated squall line largely because, once the system has become elevated, the source of parcels containing CAPE is almost entirely above 1 km (e.g., Fig. 11). These parcels need minimal vertical displacements to attain their level of free convection (which were generally located about 2 km AGL; Fig. 11,

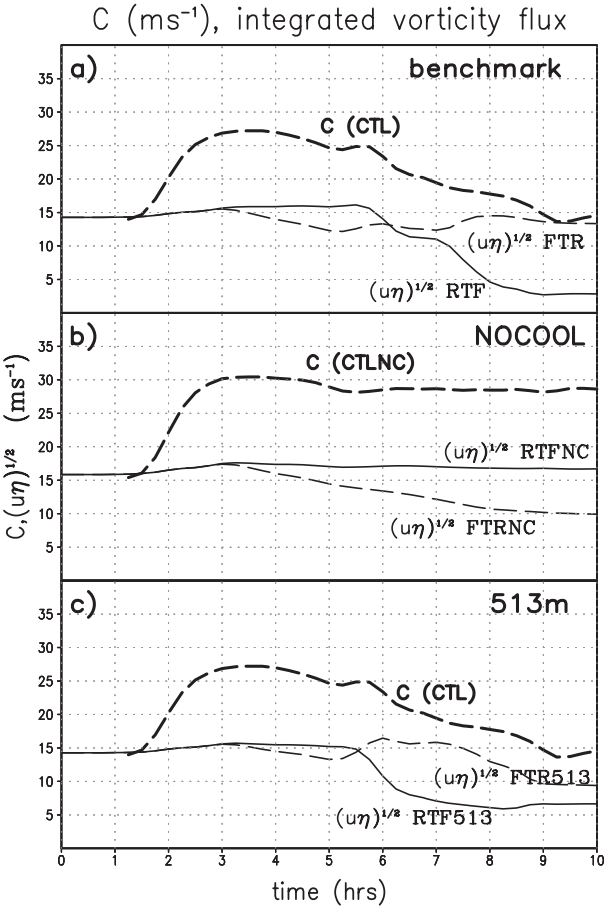

FIG. 10. Time series of C (m s^{-1}; heavy dashed line, control simulations only) and square root of $u\eta|_z$ (thin solid line for RTF jet configurations and thin dashed line for FTR jet configurations) for the (a) benchmark, (b) NOCOOL, and (c) 513m simulations. The square root of $u\eta|_z$ is shown to make the units comparable to C, and both variables are integrated over the effective inflow layer shaded in Fig. 9.

left-hand panels). Such displacements are achieved merely by isentropic ascent at the leading edge of the bore (Fig. 11), and thus convection is sustained. However, vertical shear still plays an important role in modulating this mechanism.

Schmidt and Cotton (1990) demonstrated that the amplitude of low-level gravity waves that drive squall lines in a statically stable boundary layer is controlled by the vertical wind shear, with stronger shear resulting in a higher-amplitude wave on the downshear side of the system. A similar result was found by Buzzi et al. (1991), who determined that in the presence of a low-level stable layer, the shear within the stable layer played a significant role in organizing the solitary wave driving their simulated squall line. In the present simulations there is little evidence of the gravity wave/bore below approximately 0.5 km; thus, we assume that the wave is propagating through the layer between 0.5 km and the top of the low-level stable layer (approximately 1.5 km AGL by $t = 8.5$ h). According to the studies cited above, the shear over this 0.5–1.5-km AGL layer should control the amplitude of the gravity wave/bore that drives the convective system and thus govern updraft intensity. The RTF simulation features stronger shear between 0.5 and 1.5 km AGL compared to the FTR simulation (Table 1), and this corresponds to a higher-amplitude wave and stronger low-level vertical velocities (Figs. 8b,c). This argument also explains differences in updraft shape that become evident between $t = 8.0$ and 9.0 h. In the FTR simulation, the lower-amplitude wave produces a gradual rearward slope in the isentropes, which in turn accounts for the rearward-tilted updraft evident in Fig. 8c. Conversely, the higher-amplitude wave with vertically oriented isentropes in the RTF simulation produces the nearly vertical updraft that is observed (Fig. 8c).

To summarize, the LLJ-induced changes to low-level vertical shear control updraft intensity throughout the course of our simulations. While the system remains cold pool driven, the shear within the effective inflow layer appears to explain the changes in updraft strength. From approximately $t = 3.0$–6.5 h this layer extends well below the LLJ, causing the below-jet shear to have the largest impact, favoring stronger updrafts in the RTF simulation. As the stable layer grows and approaches the level of maximum winds in the LLJ (approximately $t = 6.5$–7.5 h), the above-jet shear plays an increasingly important role, and the FTR jet then provides the most favorable condition for strong updrafts. Finally, once the squall line has become elevated and bore driven ($t = 7.5$–10.0 h), vertical motion is most clearly linked to the amplitude of the bore itself. This amplitude is controlled by the shear within the stable layer, with the stronger shear associated with the RTF jet providing the best conditions for strong lift. These arguments explain the evolution of vertical velocity observed over the course of our simulations; however, they still do account for the persistent, increased values of TUMF found in the FTR simulation. To explain this behavior, we now examine the role of the LLJ in modulating system-relative inflow.

c. *Role of changes to the storm relative inflow*

A key element in the sustenance of any MCS is a source of high-θ_e air that fuels the convective processes. In a study examining MCS dissipation (including daytime and nocturnal systems) Gale et al. (2002) found that a reduction or cessation of system-relative inflow (SRI)—or,

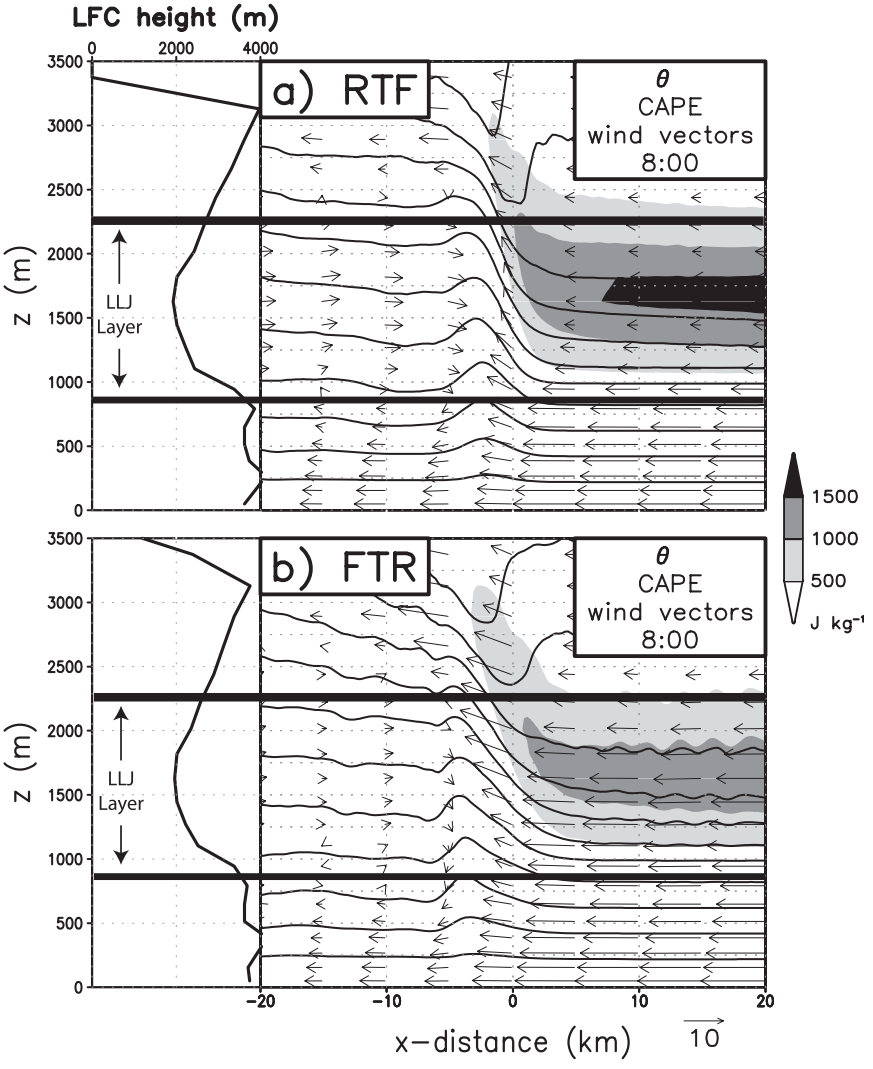

FIG. 11. Vertical cross section of along-line averaged fields for (a) RTF and (b) FTR simulations at $t = 8.0$ h: (right) potential temperature (θ; contours every 2 K starting at 294 K), wind vectors (m s^{-1}; scale vector in lower right corner), and CAPE (J kg^{-1}; shaded); (left) LFC height (m). Heavy black lines denote the top and bottom of the applied LLJ.

in the case of elevated storms, elevated system-relative inflow (ESRI)—leads to MCS weakening and eventual dissipation. They also noted that maximum values for ESRI tended to coincide temporally with the maximum LLJ intensity (approximately 0600 UTC in their dataset), suggesting that the LLJ may play a role in modulating the intensity of the ESRI. For our purposes we define SRI as flow toward the squall line within a layer containing parcels with nonzero CAPE. This distinction is important to make because as the simulated stable layer grows, air within the stable layer still flows toward the squall line. However, because of the lack of CAPE, parcels are not actually ingested by the convective updrafts. Thus, the depth of SRI changes with time, eventually becoming confined to a layer collocated with our simulated LLJ[3] (Figs. 11a,b).

The changes to system-relative inflow over time (Fig. 12a) correspond well to the changes seen in total upward

[3] It is evident in Fig. 11 that the maximum preline CAPE in the FTR simulation is about 500 J kg^{-1} lower than in the RTF. This appears to result from a larger latent heat release in the FTR simulation producing a warmer forward anvil region, which leads to a smaller area between the environmental and parcel temperature curves near the top of the column. Thus, CAPE is reduced in the integrated sense; however, inflowing parcels between 1 and 3 km and their properties up through the middle troposphere are still thermodynamically similar for both simulations.

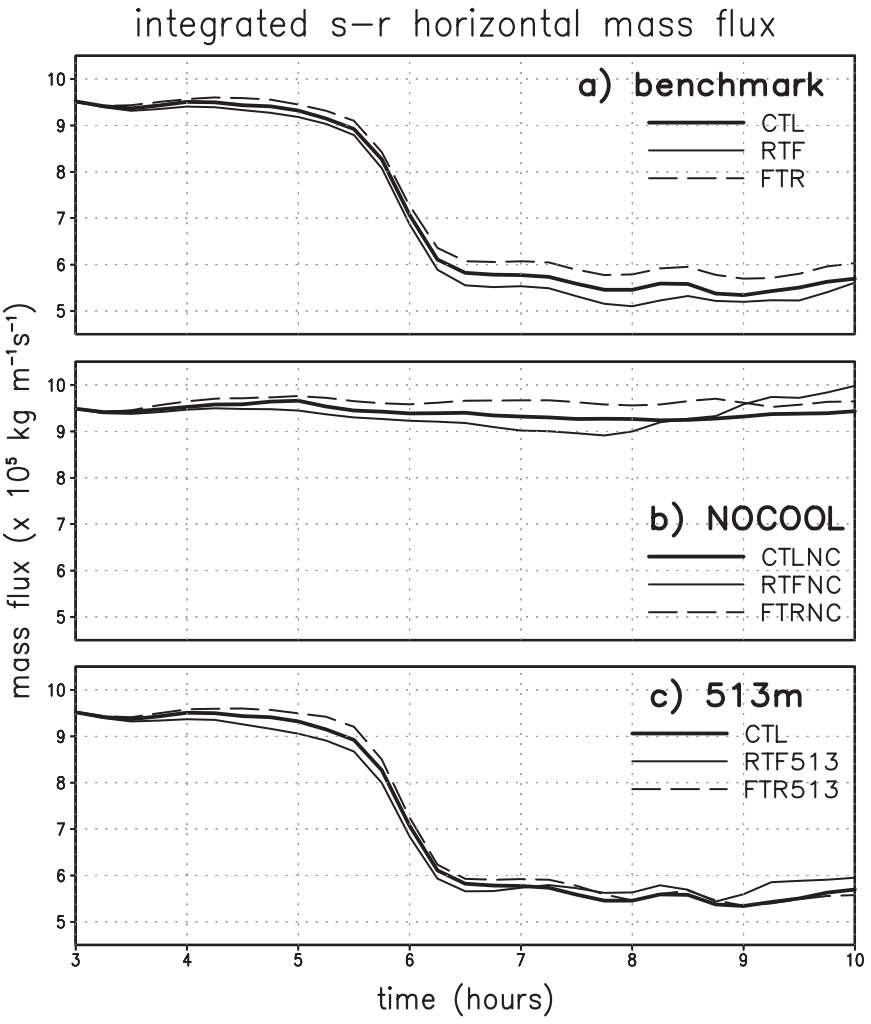

FIG. 12. Time series of vertically integrated system-relative horizontal mass flux for the (a) benchmark, (b) NOCOOL, and (c) 513m simulations. The integration is performed from the bottom of the effective inflow layer shaded in Fig. 9 to 3 km AGL in (a) and (c) and from the surface to 3 km AGL in (b). An upper bound of 3 km is chosen as it generally represents the vertical extent of air parcels containing CAPE.

mass flux (Fig. 5b), with the RTF simulation seeing a reduction starting just after the implementation of the LLJ, and the FTR an increase. These changes become particularly pronounced as the system becomes elevated after approximately $t = 7.5$ h (Fig. 12a) because of the layer of high-θ_e air becoming exclusively collocated with the LLJ (Fig. 11). These changes are directly related to the direction of the LLJ in the respective simulations. The RTF jet, directed away from the squall line, slows the background wind within the inflow layer (Fig. 11a), causing the observed decrease in SRI (Fig. 12a), while the FTR jet accelerates the background flow toward the squall line (Fig. 11b), increasing the SRI (Fig. 12a).

The variation in SRI is also evident in a trajectory analysis presented in Fig. 13. In the RTF simulation trajectories that move through the storm updraft have relatively short horizontal lengths (Fig. 13b) compared to those in the FTR simulation (Fig. 13c). The longer trajectories in the FTR simulation imply that during the 1.0-h plotting interval the updraft ingests parcels from a region that extends well ahead of the squall line. In contrast, the shorter trajectories in the RTF simulation imply that only parcels from very near the updraft are being lifted during the plotting interval. In other words, the FTR squall line is ingesting more parcels per unit time than the RTF squall line, resulting in a larger number of updraft parcels overall (Fig. 13).

These variations in SRI ultimately correspond to differences in precipitation output. As warm, moist air parcels are fluxed into the storm they ascend through the

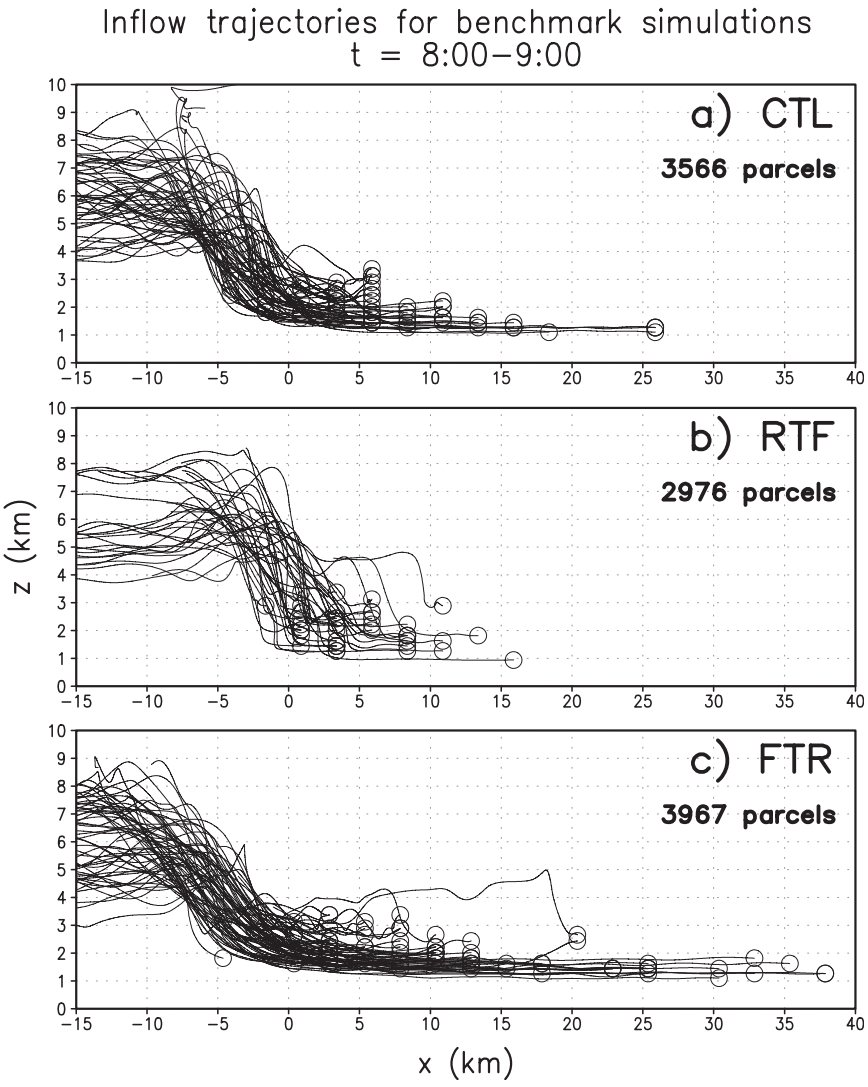

FIG. 13. Vertical cross section of parcels' trajectories plotted over 1 h between $t = 8.0$ and 9.0 h for the (a) CTL, (b) RTF, and (c) FTR simulations. The values reported below the figure label refer to the total number of parcels that passed through the updraft region of the respective squall lines during this time interval. Only a subset of these totals is plotted in the interest of clarity.

updraft region. In the FTR simulation, more air being fluxed into the storm results in more parcels being lifted, more condensation taking place per unit time, and greater hydrometeor production, ultimately resulting in an increase in precipitation output (Figs. 3g–i). The opposite was observed within the RTF simulation, wherein decreased horizontal mass flux into the storm led to fewer parcels being ingested into the storm and lifted, decreased hydrometeor production, and ultimately a decrease in precipitation (i.e., Figs. 3d–f). This reduction in inflow explains why the RTF simulation contained diminished TUMF compared to the FTR simulation despite having stronger peak updraft speeds (Figs. 5a,b).

From Fig. 3 it is clear that the addition of the LLJ caused some change in the storm motion,[4] which can also impact the SRI by changing the system-relative flow. However, the computed storm motions were still quite similar, generally ± 1 m s^{-1} compared to the CTL simulation, which is small in comparison to the 5 m s^{-1} magnitude of the imposed LLJ. Additionally, the RTF

[4] These changes appear to be due to simple advection by the LLJ. In 2D test simulations where the jet was limited to the preline region, storm motions were nearly identical for the RTF and FTR configurations.

squall line exhibits a faster motion, which would tend to increase SRI (by increasing system-relative flow toward the squall line), contrary to what is observed. Thus, the most substantial impacts of SRI upon TUMF are determined by the direction of the jet (toward or away from the system) in the preline environment.

To summarize the results of the benchmark simulations, there were two primary impacts from applying a simulated LLJ to our simulations. First, the LLJ alters the low-level wind shear profile, which controls gust front lifting as anticipated by the theory put forth by RKW. The LLJ also changes the storm-relative wind profile, impacting the strength of storm-relative inflow feeding the squall line, and with it the total upward mass flux within the squall line. These results are very much in line with the recent work of James et al. (2005), who found that low-level shear determines the vertical displacement of inflowing parcels, while storm-relative flow governs total upward mass flux. In their study, they used simulations of simple density currents to demonstrate that for constant shear, increasing the speed at which the cold pool moves (and thus the storm-relative flow) produces a concurrent increase in total upward mass flux. This is akin to our FTR simulation; however, in our case the enhanced system-relative flow is caused by the LLJ rather than by faster storm motion.

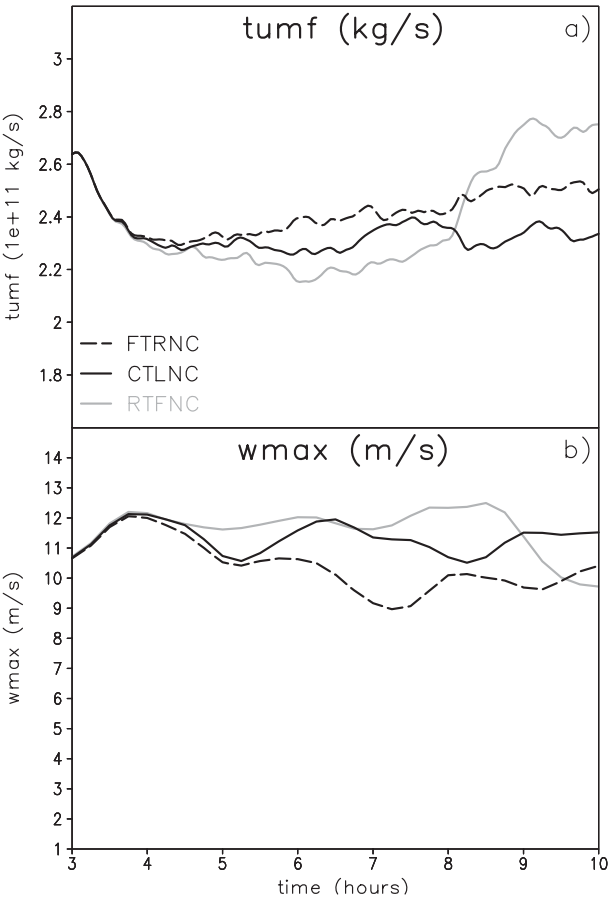

FIG. 14. As in Fig. 5, but for the NOCOOL simulations.

4. Sensitivity tests

a. Simulations without low-level cooling

The results of the previous section suggest that the impacts of the LLJ are strongly tied to the transition from surface-based to elevated convection. To separate the impact of the LLJ from the impacts of the low-level cooling, we reran our series of benchmark simulations without the cooling scheme applied. In essence, these runs simulate the impact of adding an LLJ to a squall line that remains surface based and cold pool driven throughout its lifetime. We refer to these simulations together as the ''NOCOOL'' simulations, with CTLNC, RTFNC, and FTRNC corresponding to the benchmark CTL, RTF, and FTR runs. Aside from the absence of the low-level cooling, the experimental setup remains identical to the benchmark simulations.

The NOCOOL simulations are characterized by generally steadier behavior than the benchmark simulations, at least through approximately $t = 8.0$ h (Fig. 14). This is most notable when examining $[\overline{w}]_{\max}$, as the RTFNC simulation exhibits larger values than the CTLNC run through the majority of the simulation, whereas the FTRNC run exhibits weaker values through the entirety (Fig. 14b). This is because, in the absence of low-level cooling, the layer of relevant vertical wind shear remains between approximately 0 and 1 km (the depth of the cold pool, as discussed earlier) throughout the simulation. As a result, the below-jet shear, which is stronger in the RTFNC configuration (Fig. 10b) remains important throughout the simulation. As in the benchmark simulations, the FTRNC squall line generates a larger TUMF than the CTLNC squall line throughout the run, despite now having the weaker vertical motion throughout; consistent with the concept that storm-relative inflow governs TUMF.

The primary departure from steady behavior in the NOCOOL simulations occurs within the RTFNC simulation. After about $t = 8.0$ h this simulation exhibits a marked increase in TUMF and decline in $[\overline{w}]_{\max}$ (Fig. 14). This is concurrent with a rapid increase in system speed (not shown), which is proportional to the cold pool strength, C. The increase in C overwhelms the vertical wind shear, leading to the decline in $[\overline{w}]_{\max}$. At the same time, the faster system motion increases the storm-relative flow (and thus SRI; Fig. 12b), leading to the uptick in TUMF that is observed. This is very much

in line with the findings of James et al. (2005), as discussed earlier. Thus, the NOCOOL simulations provide further evidence that (a) while the squall lines are surface-based, their behavior is controlled by the below-jet shear, and (b) TUMF is governed more by system-relative inflow than by updraft intensity.

b. 500-m jet height

As an additional sensitivity test, we present the results of a set of simulations run wherein the jet was lowered to approximately 500 m (model level $z = 513$ m). This was deemed an appropriate move because (a) in nature[5] the LLJ tends to be found at approximately 500 m and (b) by lowering the jet, we were able to assess both how the jet impacts SRI when it is removed from the layer of elevated high-θ_e air, and how the jet-induced shear impacts the squall line when the below-jet region is comparatively shallower, and as a result stabilizes faster. These simulations are referred to as the RTF513 and FTR513 simulations and will be compared to the same CTL simulation discussed previously. Aside from altering the height where the LLJ is applied, these simulations are identical to the benchmark RTF and FTR simulations. Several configurations that placed the jet higher than 1 km were tested as well; however, since these configurations removed the jet-related environmental changes from both the level of highest θ_e and strongest B', the impact on the simulated squall line was minimal and thus they will not be discussed in detail.

The 513m simulations evolve quite similarly to the benchmark simulations in terms of vertical motion through approximately 6.0 h. From $t = 3.0$ to 6.0 h, the RTF513 squall line produces larger vertical velocities than the FTR513, after which the FTR513 becomes dominant for the remainder of the simulation (Fig. 15). This transition occurs approximately 30 min sooner in the 513m simulations than in the benchmark simulations, which is to be expected, as the effective inflow layer is cut off at lower levels first and works its way upward with time. It is notable, though, that the squall lines continue to ingest parcels (and thus to flux horizontal vorticity) from below 500 m though this time period, as low-level CAPE decreases markedly and CIN grows (Fig. 9). As in the benchmark simulations, the respective periods of stronger $[\overline{w}]_{\max}$ correspond to periods of stronger $u\eta|_z$ in both simulations (Fig. 10c).

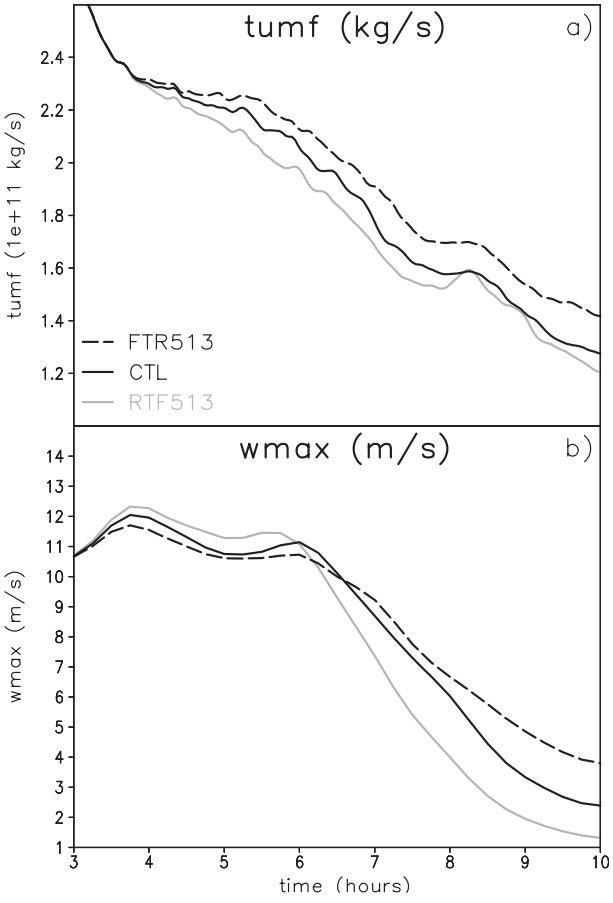

FIG. 15. As in Fig. 5, but for the FTR513, RTF513, and CTL simulations.

After $t = 7.5$ h, the behaviors of the benchmark and 513m simulations diverge as the FTR513 (RTF513) simulation continues to produce stronger (weaker) vertical velocities through the end of the simulation (e.g., Figs. 15b and 16). Because of the lower jet axis, the FTR513 simulation has favorable shear within the 0.5–1.5-km AGL stable layer, leading to a higher-amplitude gravity wave once the system becomes elevated. For this reason, FTR513 retains the strongest $[\overline{w}]_{\max}$ through the end of the 10.0-h simulation (unlike in the benchmark case; cf. Figs. 5b and 15b).

As in the previous simulations, the FTR jet configuration generates the strongest TUMF throughout the simulation. Through approximately $t = 7.5$ h both the RTF513 and FTR513 simulations have values of TUMF comparable to their benchmark simulation counterparts. However, after approximately $t = 7.5$ h the FTR513 exhibits stronger TUMF than was seen in the original

[5] As discussed in section 2, our placement of the jet at 1 km AGL for the benchmark simulations was due to this being the top of our nocturnal stable layer, which is where the jet is located in general. In nature this layer is often shallower than 1 km, thus resulting in the LLJ being found to climatologically reside around 500 m AGL. However, in the interest of including a sufficient number of model grid points within our stable layer to facilitate its gradual growth, the 1-km depth was chosen.

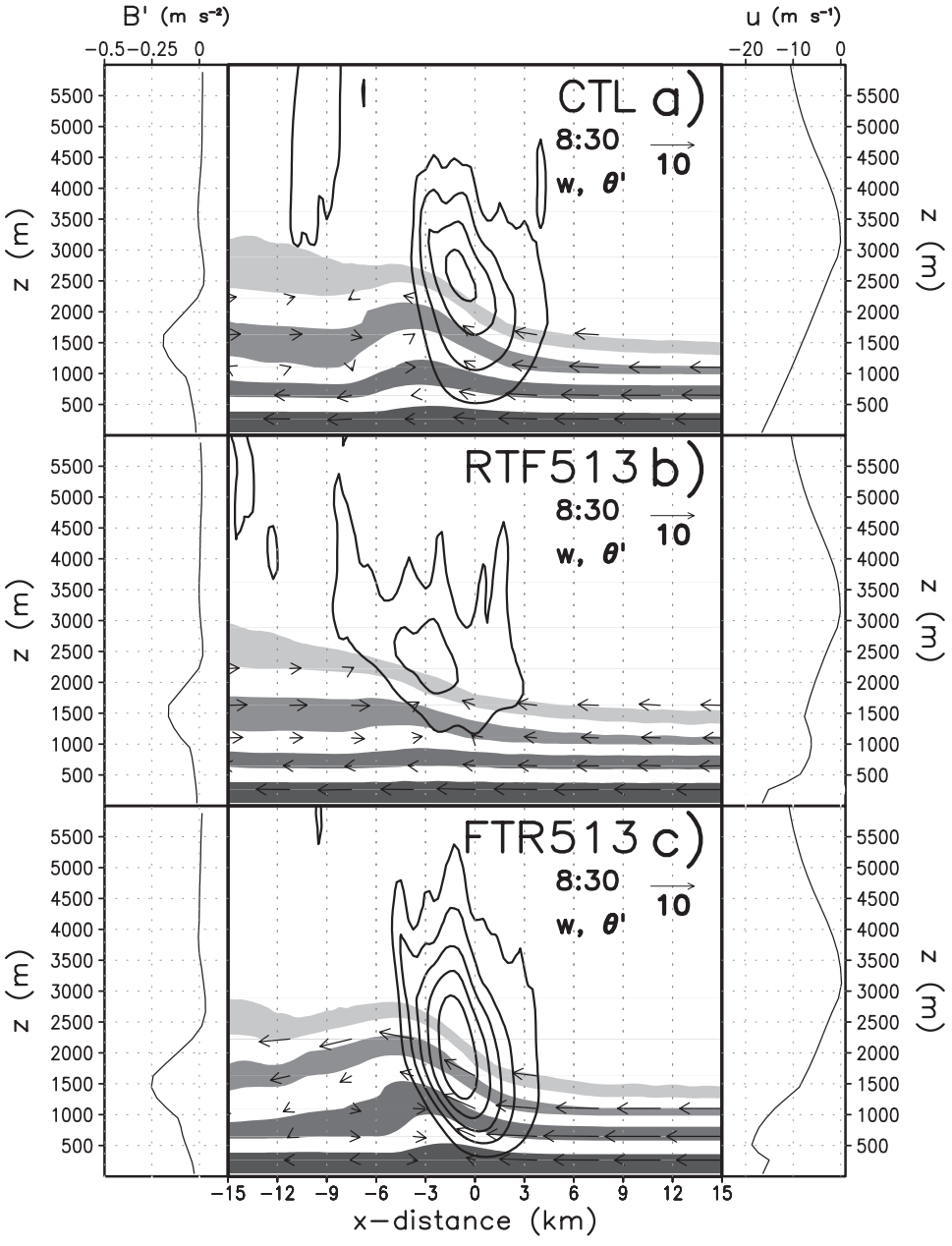

FIG. 16. As in Fig. 6, but for the CTL, RTF513, and FTR513 simulations at $t = 8.5$ h.

FTR simulation, while the RTF513 TUMF values approach those produced by the CTL simulation (Fig. 15a). It appears that when the jet is located at 513 m (within the stable layer) it ceases to have a significant influence on system-relative inflow and TUMF once the system becomes elevated. This is evident in the time series of integrated storm-relative horizontal mass flux, as the FTR513 simulation mimics the CTL during this period (Fig. 12c). This suggests that the larger TUMF associated with the FTR513 simulation after $t = 7.5$ h is likely due to the substantially larger values of $[\overline{w}]_{\max}$ that are also present.

5. Nonperiodic 3D simulations

To evaluate the effects of an LLJ on a fully three-dimensional system, a set of simulations was run using a nonperiodic configuration. Instead of focusing on a segment of an infinitely long squall line, these simulations allowed us to examine the effects of the LLJ on the

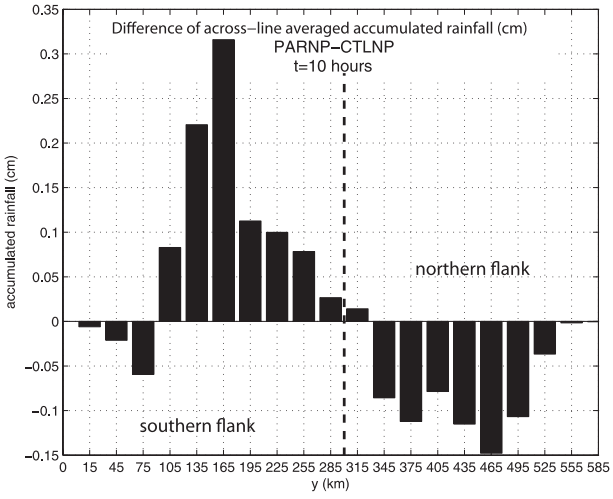

FIG. 17. Difference plot of across-line (east–west) averaged accumulated rainfall (cm) comparing PARNP and CTLNP simulations (PARNP − CTLNP). The data are grouped into 30-km-wide (north–south) bins that are centered on the points shown along the horizontal axis. The dashed vertical line denotes the center of the squall line at $y = 300$ km.

system as a whole, including the development of 3D asymmetries along the line. The primary changes to the model configuration for these simulations consisted of using an open-y lateral boundary condition and a larger domain in the y direction (increased from 60 to 600 km) to allow for a sufficiently long convective line while keeping it away from the lateral boundaries. Additionally, a coarser horizontal grid spacing (dx and dy were increased from 250 to 500 m) was utilized to keep run times manageable given the larger domain. The squall line was initiated using a warm line thermal as before, in this case limited to a y length of 200 km and centered at $y = 300$ km. The three benchmark simulations (CTLNP, RTFNP, and FTRNP) as well as the line-parallel jet simulation (PARNP) were all rerun using this configuration (Fig. 2b).

In general the impact of the RTF and FTR jets in the nonperiodic configuration was the same as for the periodic simulations, with the FTR creating more precipitation output and the RTF less precipitation. The impact of adding the line-parallel jet is subtle, with the CTLNP and PARNP simulations maintaining similar characteristics through 8.0 h. After this point, the two diverge slightly, with the PARNP simulation featuring an increase (decrease) in precipitation along its southern (northern) flank compared to the CTLNP (Fig. 17). This result is in line with those from the periodic simulations discussed earlier. In this case, the southern half of the PARNP squall line is experiencing an effect akin to an FTR jet, with an increase in precipitation due to an increase in horizontal mass flux into the system. At the same time, the northern half of the PARNP squall line is experiencing an effect akin to the RTF jet, with a reduction in storm-relative inflow leading to the observed decrease in precipitation output. Thus, the primary impact of the addition of a line-parallel LLJ to a completely 3D simulated system is an alteration of the precipitation distribution around the storm. Overall, though, the impact is subtle, likely owing to the deep-layer westerly shear and homogeneous background environment favoring continued development along the generally north–south-oriented bore. The overall system motion continues to be eastward because of the mean westerly winds and system propagation in the downshear direction. In other words, storm motion is primarily governed by the base state wind profile, whereas the effect of the LLJ is to locally modulate the storm-relative inflow.

6. Discussion

This work set out with the goal of examining the impacts of adding a low-level jet to an elevated squall line. Two primary impacts were identified: 1) the LLJ changes the vertical shear, resulting in changes to updraft intensity in the simulated squall lines and 2) the LLJ modulates the intensity of the system-relative inflow within the jet layer, with the orientation of the jet governing whether SRI is increased or decreased. In general, the shear impacts modulated vertical velocities within our simulated squall line, while changes in storm-relative inflow impacted total upward mass flux and precipitation output. Both of these impacts were affected by the transition from surface-based to elevated convection over the life of the squall line. While the system was surface based, the shear below the jet appeared to have the largest impact (Fig. 18a). As the system became elevated the shear above the jet became increasingly important, while low-level CAPE decreased and the strongest B' shifted upward due to low-level stabilization (Fig. 18b). Once the system became completely elevated, the forcing became that of a bore, and the vertical shear ceased to directly impact low-level lifting via density current–shear dynamics. Instead it appeared to control the amplitude of the gravity wave/bore (Fig. 18c). Storm-relative inflow impacts also varied with system evolution, with LLJ-induced changes to SRI becoming more pronounced as the system became elevated and the layer of highest-θ_e air was limited to that of the LLJ.

Fritsch et al. (1994) and Schumacher (2009) have also investigated the impact of an LLJ on the RKW cold pool–shear balance. As in the present work, both studies found that an LLJ oriented toward the system (our FTR configuration) resulted in unfavorable shear (in the RKW

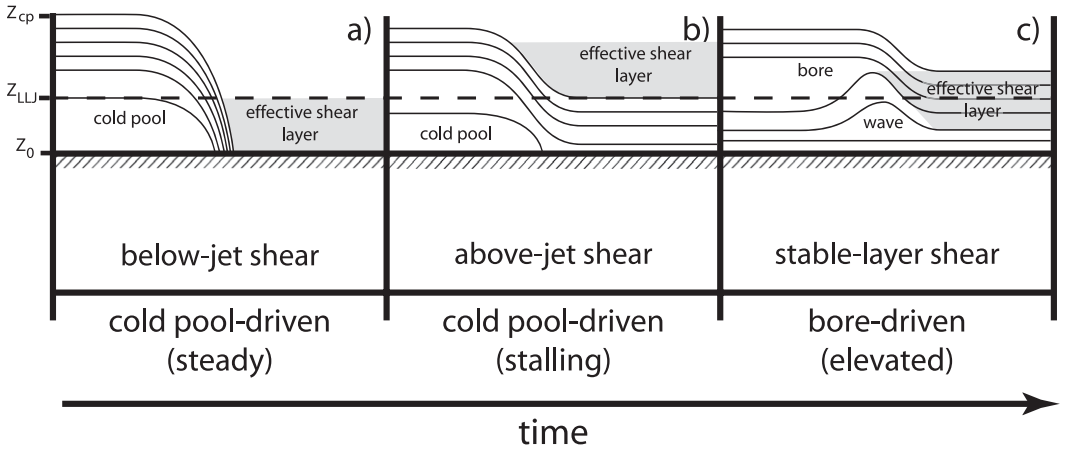

FIG. 18. Schematic diagram illustrating the key layers of vertical wind shear participating in the cold pool–shear balance relative to the height of the maximum LLJ winds (Z_{LLJ}; heavy dashed line) and cold pool depth (Z_{cp}) over time. Thin lines are representative isentropes that define the cold pool/bore, and the shaded area represents the layer of vertical shear. The evolution is broken into three periods corresponding to different points in the squall line's evolution.

sense) below the jet, inhibiting lifting, and favorable shear above the jet, promoting stronger lifting. In these studies additional low-level lifting, in the form of isentropic ascent associated with a mesoscale convective vortex (MCV), effectively compensated for the less favorable RKW condition below the jet. Once parcels were lifted sufficiently through this mechanism, they were accelerated upward by the more favorable RKW conditions in the above-jet layer. Thus, in nature additional factors can compensate for unfavorable shear associated with a low-level jet. However, as the present results suggest, when cold-pool lifting is dominant, the shear associated with the layer of high-θ_e inflow is of primary importance. In light of this, for the case of vertically varying cold pool buoyancy and environmental horizontal vorticity flux, we suggest that the commonly applied ''RKW balance'' concept may be most applicable to an ''effective inflow layer,'' which we define as follows. The predominant contribution to the integrated horizontal vorticity tendency emerges from a layer defined by the union of (a) potentially buoyant inflow parcels (CAPE > 0 J kg^{-1} and small CIN) with (b) substantial negative buoyancy (and hence baroclinicity) in the cold pool. In the present simulations, even though the total shear over the entire depth of the cold pool (i.e., over 0–2.5 km AGL) changed very little, the flux of horizontal vorticity within the effective inflow layer described the differences among the simulated vertical velocities quite well.

The findings presented herein also suggest that changes to the system-relative inflow, or the rate at which parcels are ingested by a squall line, can have a more significant impact on total upward mass flux and precipitation output than maximum updraft strength [much as shown by James et al. (2005)]. Conditions that favored enhanced flow toward the storm universally saw an uptick in total upward mass flux. Perhaps the most dramatic example of this was seen in the RTFNC simulation, where an increase in system speed, and thus system-relative flow, simultaneously resulted in both a precipitous drop in $[\overline{w}]_{max}$ and an increase in upward mass flux (Fig. 14). Additionally, all of the simulations using the FTR jet configuration demonstrated an increase in TUMF that began just after the LLJ started to develop and lasted for the duration of the simulation. This can make it challenging to quantify squall line intensity, as two common metrics, updraft velocity and total upward mass flux, do not always parallel one another.

One of the motivations for the PARNP simulation was to provide a comparison to the work of Corfidi et al. (1996) and Corfidi (2003), who emphasized the role of the LLJ in governing squall line motion. Our results indicate that enhanced precipitation does appear to occur on the flank of the storm that is interacting with the LLJ (in our case the southern flank; Fig. 17). However, in our simulations no significant change in storm motion toward the direction of the LLJ was observed. Rather, the squall line appeared to continue to move in the base-state downshear direction (eastward), apparently because of lifting along the downshear edge of the bore and advection by the mean westerlies in our wind profile. This is in agreement with the findings of Corfidi (2003) that for cold-pool-driven (or, in this case, bore-driven) squall lines, the direction of cold pool (bore) motion better represents the propagation component of the squall line's motion. It is possible, however that in

cases of weaker westerly shear, or a stronger jet, the LLJ may have a more significant effect on altering storm motion, as its impacts would be larger in a relative sense. Our simulations only continued for 2.0 h following the jet reaching its full intensity. Perhaps a longer period of influence by the jet would have had a more significant impact on storm motion. Additionally, in nature the LLJ is often longitudinally narrow and is the sole region of elevated instability, which would tend to favor propagation into the jet, as that is where the most instability to fuel new cell development would be located.

As a final note, we emphasize that the time and duration of these evolutionary stages (e.g., in Fig. 18) may be somewhat different in nature. We allowed artificial low-level cooling to proceed at a constant rate indefinitely. In nature, where the nocturnal temperature decrease varies in rate and total magnitude from day to day, squall lines may reside in any one of these three stages (e.g., Fig. 18) for much longer or shorter periods.

7. Conclusions

A series of numerical simulations has been performed to evaluate the effects of the addition of a low-level jet on a simulated squall line that is subjected to low-level cooling. The jet changes the squall line in two ways: 1) by altering the low-level wind shear and thus modulating low-level lifting and 2) by modulating the intensity of the storm-relative inflow. Overall, changes to the vertical shear have the largest impact on vertical velocities within the squall line. To this end, below-jet shear appears to have the most significant impacts while the system is surface-based, with above-jet shear having a larger impact as the system becomes elevated. Once the system becomes entirely bore driven, vertical shear continues to play a role in modulating vertical motion; however it does so by impacting the amplitude of the gravity wave/bore within the low-level stable layer. The exact details of the process remain unclear, although it is possible, as speculated by Schmidt and Cotton (1990), that it could be similar to the vorticity balance discussed by RKW. Future investigation to this end could be enlightening. The changes to system-relative inflow, on the other hand, impacted total upward mass flux and precipitation output, with a jet directed toward the squall line favoring enhancement of these fields and a jet directed away from the squall line favoring a reduction. The impacts of the system-relative inflow were more dramatic once the stable layer had deepened and the high-θ_e air was entirely collocated with the LLJ.

Acknowledgments. The authors thank George Bryan of NCAR for providing the numerical model used to run these simulations, as well as for some helpful suggestions regarding this work. Computing resources to run the simulations were provided by Renaissance Computing Institute in Chapel Hill, NC. We would also like to thank William Gallus for comments on a conference presenation about this research, and Stan Trier, Russ Schumacher, and Alexandre Fierro for their insightful reviews that greatly improved the original manuscript. Finally we thank the members of the Convective Storms Group at North Carolina State for helpful comments and assistance throughout the course of this project. This research was supported by NSF Grant ATM-0552154.

APPENDIX

Relative Humidity Correction in P08

As noted in section 2, the relative humidity (RH) correction described by P08 was not applied consistently in his simulations, nor was it optimally designed. This appendix discusses the nature of the problem and the impacts on the results of P08.

a. Nature of the deficiency in P08

One of the primary problems with the way that P08 instituted the RH $\leq$ 0.98 correction is that the technique can lead to surprisingly low RH values in the simulated systems' postline regions. After several hours of artificial cooling, wavelike vertical displacements began to emerge in the stable low-level flow of P08's simulations (see, e.g., the isentropes in Figs. 12 and 16 of P08). As a part of this wavelike flow branch, inflowing air parcels would first ascend several hundreds of meters and then would subside again. The problem with the P08 RH correction is illustrated by considering an initially saturated (or nearly saturated) air parcel undergoing such a vertical excursion. In nature, when supersaturation occurs because of the parcel's vertical displacement, cloud droplets are formed. Such droplets remain in the airstream and are subsequently evaporated during the parcel's downward displacement, yielding a parcel whose final characteristics are very similar to those with which it began. However, if the P08 RH correction is applied, the parcel's RH is reset to 0.98 at the apex of its upward displacement, with the subsequent removal of any excess cloud water. The parcel therefore is subsaturated during its downward displacement, yielding a RH that may be as low as 0.80 once it has returned to its original altitude.

In short, an unintended consequence of the P08 scheme's implementation was that the RH correction in some cases removed condensate that should have been

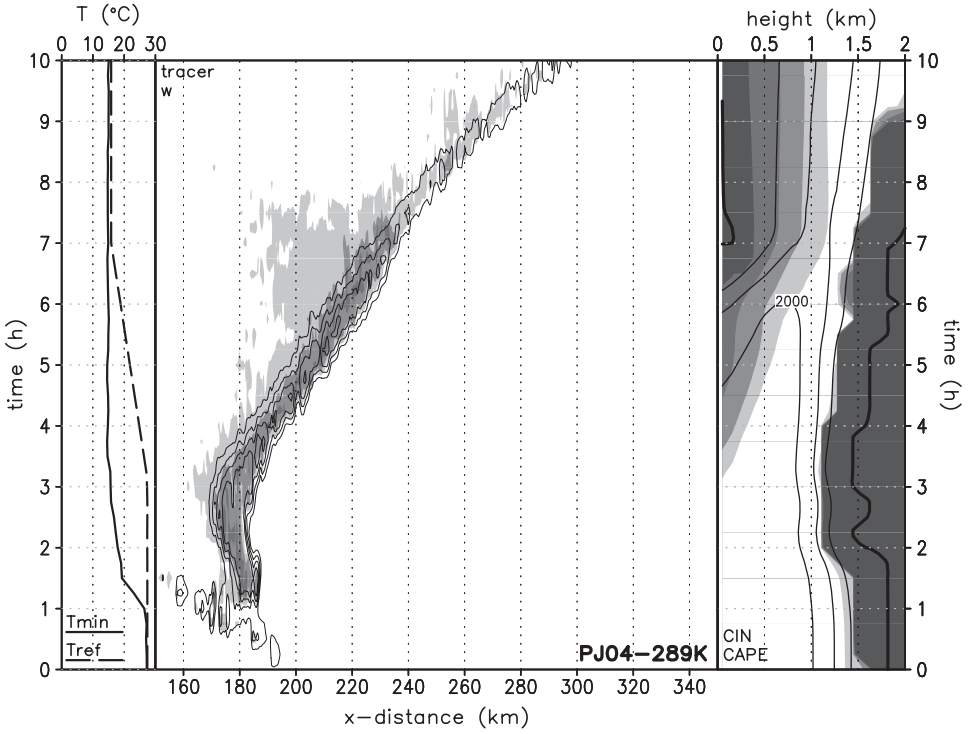

FIG. A1. As in Fig. 4, but for our rerun of the PJ04 289-K simulation. This figure is directly comparable to Fig. 11 of P08.

present because of the grid-scale processes in the model. Without delving too deeply into the various iterations that led up to the original P08 RH correction, it is clear that it has undesirable side effects. As explained in section 2, in the present revised version the artificial cooling routine is applied after the model microphysical parameterization, allowing the model to treat moist processes associated with the resolved motions first. Then, when the artificial cooling is added, only supersaturation and condensation caused specifically by the artificial cooling are removed. Thus, in the preceding thought experiment, the grid-scale ascent will produce cloud water that remains in the low-level flow as it proceeds into the postline region, leading to much more realistic postline RH values.

The negative consequence of the unrealistically depressed low-level RH values in P08 is that additional low-level evaporative cooling occurs when the squall line's precipitation falls into the subsaturated airstream. In other words, the convective outflow ends up being somewhat stronger than it should be. There are also some small impacts on the vertical force balance because the artificial removal of (legitimately produced) cloud water removes hydrometeor loading, meaning that parcel buoyancy in the low levels was slightly less negative than it should realistically have been; however, the hydrometeor loading in this region of the P08 squall lines was actually quite small compared to the negative thermal buoyancy.

b. Impacts on the conclusions of P08

We reran all of the P08 simulations, uniformly applying the revised (improved) cooling and RH correction code. Our newly rerun simulations differ in some details but continue to uphold the principal conclusions summarized on p. 1339 of P08. Much of the discussion in P08 followed from his DEEP-unlim run, which used the same environment and cooling profile as our current study. Interested readers may compare Figs. 4, 6a, and 11 in the present article with Figs. 5–9 in P08 to verify just how little is changed by the revised cooling–RH scheme. Indeed, very few of the plots from the new simulations are notably different from those that appear in P08. What follows are the exceptions.

First off, in the reruns using the PJ04 midlatitude MCS sounding and limited cooling, the simulated squall lines are less able to continue ingesting low-level air as time passes. In our rerun, we found that the system's outflow was somewhat weaker (owing to the revised RH correction discussed above). As a consequence, the PJ04 289-K squall line was much weaker and barely ingested any low-level air after roughly $t = 7.5$ h (Fig. A1). A similar decrease in intensity also occurred when we reran

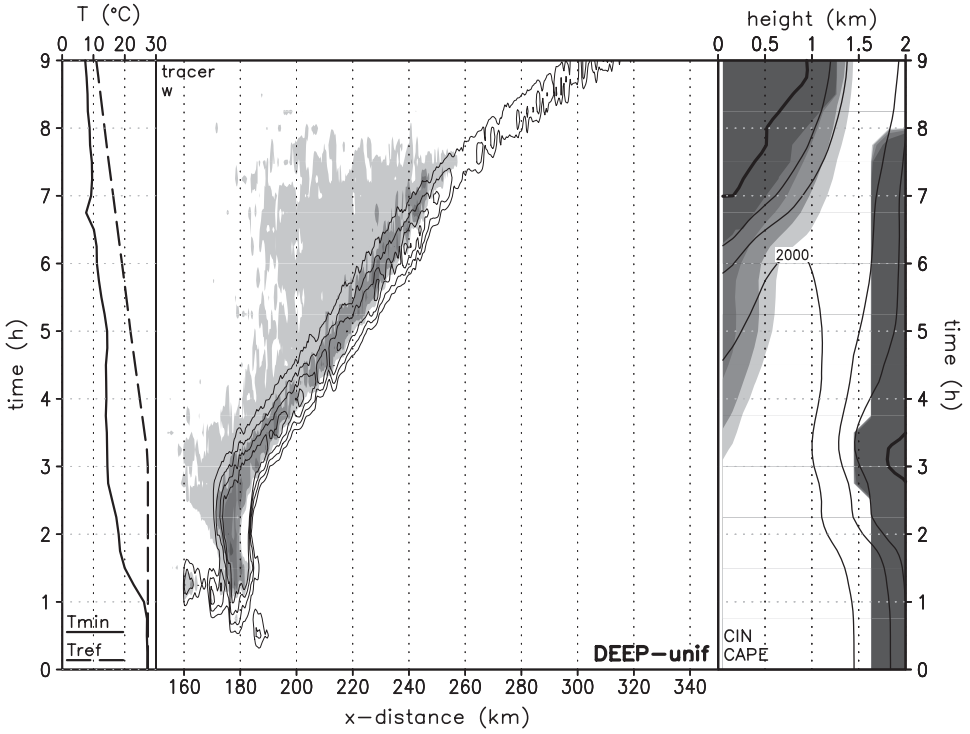

FIG. A2. As in Fig. 4, but for our rerun of the DEEP-unif simulation. This figure is directly comparable to Fig. 15 of P08.

the PJ04 287-K (i.e., with 14 K of cooling) simulation, such that the convection dissipated after 9.0 h (not shown).

There were also noticeable differences in the rerun of P08's DEEP-unif run, which utilized the sounding from the present study but in which the 3 K h^{-1} cooling was uniformly applied to every grid point below 1 km AGL (i.e., including the cold pool, not just the environment). In our rerun of the DEEP-unif case (Fig. A2), the system remained surface based for a longer period of time (through $t = 7.5$ h, as compared to about 6.5 h in P08). The rerun of DEEP-unif also displayed a much slower forward speed in its later stages, including some evidence of slowing/stalling during the period $t = 5.5$–7.5 h (Fig. A2). These changes are attributable to two effects. First, once again the system's cold pool density current was less cold (cf. our Fig. A2 to P08's Fig. 15) because of the revised RH correction, which enabled the system to slow (i.e., a stalling phase became possible). Second, because the revised RH correction lessened the amount of evaporative cooling in the vicinity of the system's developing bore, it took much longer for the bore to develop significant amplitude and outrun the surface density current.

Most other differences were minor. In short, it appears that the physical interpretations presented by P08 are robust but that the system speeds and cold pool temperatures were overdone in some cases because of the poorly implemented RH correction.

REFERENCES

Anderson, C. J., and R. W. Arritt, 1998: Mesoscale convective complexes and persistent elongated convective systems over the United States during 1992 and 1993. *Mon. Wea. Rev.,* **126,** 578–599.

Arritt, R. W., T. D. Rink, M. Segal, D. P. Todey, and C. A. Clark, 1997: The Great Plains low-level jet during the warm season of 1993. *Mon. Wea. Rev.,* **125,** 2176–2192.

Augustine, J. A., and F. Caracena, 1994: Lower tropospheric precursors to nocturnal MCS development over the central United States. *Wea. Forecasting,* **9,** 116–135.

Bluestein, H. B., and M. H. Jain, 1985: Formation of mesoscale lines of precipitation: Severe squall lines in Oklahoma during the spring. *J. Atmos. Sci.,* **42,** 1711–1732.

Bonner, W. D., 1968: Climatology of the low-level jet. *Mon. Wea. Rev.,* **96,** 833–850.

Braun, S. A., and W.-K. Tao, 2000: Sensitivity of high-resolution simulations of Hurricane Bob (1991) to planetary boundary layer parameterization. *Mon. Wea. Rev.,* **128,** 3941–3961.

Bryan, G. H., and M. J. Fritsch, 2002: A benchmark simulation for moist nonhydrostatic numerical models. *Mon. Wea. Rev.,* **130,** 2917–2928.

——, J. C. Knievel, and M. D. Parker, 2006: A multimodel assessment of RKW theory's relevance to squall-line characteristics. *Mon. Wea. Rev.,* **134,** 2772–2792.

Buzzi, A., M. Fantini, and G. Lippolis, 1991: Quasi-stationary organized convection in the presence of an inversion near the

surface: Experiments with a 2-D numerical model. *Meteor. Atmos. Phys.,* **45,** 75–86.

Carbone, R. E., J. W. Conway, N. A. Crook, and M. W. Moncrieff, 1990: The generation and propagation of a nocturnal squall line. Part I: Observations and implications for mesoscale predictability. *Mon. Wea. Rev.,* **118,** 26–49.

Corfidi, S. F., 2003: Cold pools and MCS propagation: Forecasting the motion of downwind-developing MCSs. *Wea. Forecasting,* **18,** 997–1017.

——, J. H. Merritt, and J. M. Fritsch, 1996: Predicting the movement of mesoscale convective complexes. *Wea. Forecasting,* **11,** 41–46.

Cotton, W. R., M. S. Lin, R. L. McAnelly, and C. J. Tremback, 1989: A composite model of mesoscale convective complexes. *Mon. Wea. Rev.,* **117,** 765–783.

Doswell, C. A., III, H. E. Brooks, and R. A. Maddox, 1996: Flash flood forecasting: An ingredients-based methodology. *Wea. Forecasting,* **11,** 560–581.

Dudhia, J., M. W. Moncrieff, and D. W. K. So, 1987: The two-dimensional dynamics of West African squall lines. *Quart. J. Roy. Meteor. Soc.,* **113,** 121–146.

Fritsch, J. M., R. J. Kane, and C. R. Chelius, 1986: The contribution of mesoscale convective weather systems to the warm-season precipitation in the United States. *J. Climate Appl. Meteor.,* **25,** 1333–1345.

——, J. D. Murphy, and J. S. Kain, 1994: Warm core vortex amplification over land. *J. Atmos. Sci.,* **51,** 1780–1807.

Gale, J. J., W. A. Gallus Jr., and K. A. Jungbluth, 2002: Toward improved prediction of mesoscale convective system dissipation. *Wea. Forecasting,* **17,** 856–872.

Gallus, W. A., Jr., N. A. Snook, and E. V. Johnson, 2008: Spring and summer severe weather reports over the Midwest as a function of convective mode: A preliminary study. *Wea. Forecasting,* **23,** 101–113.

Goodman, S. J., and D. R. MacGorman, 1986: Cloud-to-ground lightning activity in mesoscale convective complexes. *Mon. Wea. Rev.,* **114,** 2320–2328.

Helfand, H. M., and S. D. Schubert, 1995: Climatology of the simulated Great Plains low-level jet and its contribution to the continental moisture budget of the United States. *J. Climate,* **8,** 784–806.

Higgins, R. W., Y. Yao, E. S. Yarosh, J. E. Janowiak, and K. C. Mo, 1997: Influence of the Great Plains low-level jet on summertime precipitation and moisture transport over the central United States. *J. Climate,* **10,** 481–507.

James, R. P., J. M. Fritsch, and P. M. Markowski, 2005: Environmental distinctions between cellular and slabular convective lines. *Mon. Wea. Rev.,* **133,** 2669–2691.

Kincer, J. B., 1916: Daytime and nighttime precipitation and their economic significance. *Mon. Wea. Rev.,* **44,** 628–633.

Lin, Y.-L., R. D. Farley, and H. D. Orville, 1983: Bulk parameterization of the snow field in a cloud model. *J. Climate Appl. Meteor.,* **22,** 1065–1092.

Maddox, R. A., 1980: Mesoscale convective complexes. *Bull. Amer. Meteor. Soc.,* **61,** 1374–1387.

——, 1983: Large-scale meteorological conditions associated with midlatitude mesoscale convective complexes. *Mon. Wea. Rev.,* **111,** 1475–1493.

Means, L. L., 1952: On thunderstorm forecasting in the central United States. *Mon. Wea. Rev.,* **80,** 165–189.

Mitchell, M. J., R. W. Arritt, and K. Labas, 1995: A climatology of the warm season Great Plains low-level jet using wind profiler observations. *Wea. Forecasting,* **10,** 576–591.

Parker, M. D., 2008: Response of simulated squall lines to low-level cooling. *J. Atmos. Sci.,* **65,** 1323–1341.

——, and R. H. Johnson, 2004: Structures and dynamics of quasi-2D mesoscale convective systems. *J. Atmos. Sci.,* **61,** 545–567.

Pitchford, K. L., and J. London, 1962: The low-level jet as related to nocturnal thunderstorms over Midwest United States. *J. Appl. Meteor.,* **1,** 43–47.

Rotunno, R., J. B. Klemp, and M. L. Weisman, 1988: A theory for strong, long-lived squall lines. *J. Atmos. Sci.,* **45,** 463–485.

Schmidt, J. M., and W. R. Cotton, 1990: Interactions between upper and lower tropospheric gravity waves on squall line structure and maintenance. *J. Atmos. Sci.,* **47,** 1205–1222.

Schumacher, R. S., 2009: Mechanisms for quasi-stationary behavior in simulated heavy-rain-producing convective systems. *J. Atmos. Sci.,* **66,** 1543–1568.

——, and R. H. Johnson, 2005: Organization and environmental properties of extreme-rain-producing mesoscale convective systems. *Mon. Wea. Rev.,* **133,** 961–976.

——, and ——, 2009: Quasi-stationary, extreme-rain-producing convective systems associated with midlevel cyclonic circulations. *Wea. Forecasting,* **24,** 555–574.

Song, J. K., R. L. Liao, R. L. Coulter, and B. M. Lesht, 2005: Climatology of the low-level jet at the southern Great Plains atmospheric boundary layer experiments site. *J. Appl. Meteor.,* **44,** 1593–1606.

Tollerud, E. I., and Coauthors, 2008: Mesoscale moisture transport by the low-level jet during the IHOP field experiment. *Mon. Wea. Rev.,* **136,** 3781–3795.

Trier, S. B., and D. B. Parsons, 1993: Evolution of environmental conditions preceding the development of a nocturnal mesoscale convective complex. *Mon. Wea. Rev.,* **121,** 1078–1098.

——, C. A. Davis, D. A. Ahijevych, M. L. Weisman, and G. H. Bryan, 2006: Mechanisms supporting long-lived episodes of propagating nocturnal convection within a 7-day WRF model simulation. *J. Atmos. Sci.,* **63,** 2437–2461.

Tuttle, J. D., and C. A. Davis, 2006: Corridors of warm season precipitation in the central United States. *Mon. Wea. Rev.,* **134,** 2297–2317.

Wallace, J. M., 1975: Diurnal variations in precipitation and thunderstorm frequency over the conterminous United States. *Mon. Wea. Rev.,* **103,** 406–419.

Weisman, M. L., and R. Rotunno, 2004: ''A theory for strong long-lived squall lines'' revisited. *J. Atmos. Sci.,* **61,** 361–382.

——, J. B. Klemp, and R. Rotunno, 1988: Structure and evolution of numerically simulated squall lines. *J. Atmos. Sci.,* **45,** 1990–2013.

Wetzel, P. J., W. R. Cotton, and R. L. McAnelly, 1983: A long-lived mesoscale convective complex. Part II: Evolution and structure of the mature complex. *Mon. Wea. Rev.,* **111,** 1919–1937.

Whiteman, C. D., X. Bian, and S. Zhong, 1997: Low-level jet climatology from enhanced rawinsonde observations at a site in the southern Great Plains. *J. Appl. Meteor.,* **36,** 1363–1376.